VARIABILITY OF THE SOUTH PACIFIC CONVERGENCE ZONE AND ITS INFLUENCE ON THE GENERAL ATMOSPHERIC CIRCULATION

A Thesis
Presented to
The Academic Faculty

by

Matthew Widlansky

In Partial Fulfillment
of the Requirements for the Degree
Master's of Science in the
School of Earth and Atmospheric Sciences

Georgia Institute of Technology
December 2007

VARIABILITY OF THE SOUTH PACIFIC CONVERGENCE ZONE AND ITS INFLUENCE ON THE GENERAL ATMOSPHERIC CIRCULATION

Approved by:

Dr. Peter J. Webster, Advisor
School of Earth and Atmospheric Sciences
Georgia Institute of Technology

Dr. Emanuele Di Lorenzo
School of Earth and Atmospheric Sciences
Georgia Institute of Technology

Dr. Rong Fu
School of Earth and Atmospheric Sciences
Georgia Institute of Technology

Date Approved: November 13, 2007

ACKNOWLEDGEMENTS

Guidance from my advisor, Dr. Peter J. Webster, developed the foundation for ideas contained in this thesis and supported it through completion. I am also greatly appreciative of Drs. Emanuel Di Lorenzo and Rong Fu for their participation as members of my thesis committee.

Special thanks are owed to the other members of the Webster research group and to those within the School of Earth and Atmospheric Sciences at the Georgia Institute of Technology for providing an invaluable education. I am also especially grateful for the thorough editorial advice from Jason Furtado and Mark Jelinek. The opportunity to study and work with all of these scientists has been an honor. Encouragement, patience, and endless support from family and friends allowed me to develop this thesis from a lifelong interest in weather.

TABLE OF CONTENTS

LIST OF FIGURES

LIST OF ABBREVIATIONS

CDC	Climate Diagnostics Center
DJF	December, January, February
ENSO	El Niño-Southern Oscillation
EOF	Empirical Orthogonal Analysis
GCM	General Circulation Model
ITCZ	Intertropical Convergence Zone
JJA	June, July, August
MAM	March, April, May
MCS	Mesoscale Convective System
MIMI	Meteorological Observations, Andover, MA
MJO	Madden-Julian Oscillation
NCAR	National Center for Atmospheric Research
NCEP	National Centers for Environmental Prediction
NH	Northern Hemisphere
NOAA	National Oceanic and Atmospheric Administration
OI	Optimum Interpolation
OLR	Outgoing Longwave Radiation
PC	Principal Component
SACZ	South Atlantic Convergence Zone
SICZ	South Indian Convergence Zone
SLP	Sea-Level Pressure

SST	Sea Surface Temperature
SPCZ	South Pacific Convergence Zone
SH	Southern Hemisphere
SD	Standard Deviation
TC	Tropical Cyclone

SUMMARY

Intense atmospheric convection associated with the South Pacific Convergence Zone (SPCZ) significantly impacts basin-scale circulation patterns over the Pacific. We explore dynamical processes which foster changes in convection along the convergence zone. These forcings include strong moisture convergence and accumulation of wave energy in the boundary layer, as well as dynamical instability associated with moderate cross-equatorial wind bursts. A focus is applied to observing the dominant modes of variability on synoptic to intraseasonal timescales using a combination of satellite observations and NCEP reanalysis data. Accumulation of energy, due to negative stretching deformation, occurs with both tropical and extratropical modes suggesting that the SPCZ is an artifact of wide ranging modes. Signals of the dominant modes (inferred from fields of outgoing longwave radiation: OLR) are isolated using bandpass filtering techniques, which are then mapped in space and time using Principal Components from Empirical Orthogonal Function analyses.

Variability of convective systems in the SPCZ is found to be significantly correlated with changes in the regional Hadley Circulation and the Pacific Walker cell. This co-variability presents the possibility of important teleconnection routes between the tropical West and East Pacific, as well as with the mid-latitude regions of the Northern and Southern Hemispheres. We test these interaction hypotheses by developing composites of the circulation patterns using dates of maximum convection events (regions of minimum OLR) in the SPCZ. Intensities of the large-scale circulations are measured using observations of stream function mass fluxes. Results suggest that deep

convection maxima (minima) are associated with an increase (decrease) in the Walker Circulation. It is also illustrated how off-equatorial convection anomalies in the subtropical portion of the SPCZ may induce changes to the Hadley Circulation. Interactions with the zonal (Walker) and meridional (Hadley) circulations appear to have important consequences on the ability for wave energy to propagate through the tropical Pacific atmosphere. Examples include Northern Hemisphere cross-equatorial teleconnections through the "Westerly Wind Duct" in the upper branch of the Walker circulation and Rossby wave trains in the SPCZ, which may be partially governed by characteristics of the regional Hadley circulation.

CHAPTER 1

INTRODUCTION

The South Pacific Convergence Zone (SPCZ), first described by Streten (1973) and Trenberth (1976), is a region of widespread cloud cover and precipitation extending in a southeast direction from New Guinea into the Southern Hemisphere (SH) mid-latitudes. Climatological studies of the region (e.g., Vincent 1994; Karoly and Vincent 1999; and Cocks 2003) have found pronounced spatial differences in the SPCZ between the tropical, subtropical, and mid-latitude regions. Tropical convection is oriented zonally, is highly correlated with the warmest SSTs, and often is triggered by strong boundary layer convergence (Vincent 1994). Further south in the subtropics and mid-latitudes, the SPCZ becomes more diagonally oriented and is influenced primarily by baroclinic-type disturbances. Surface layer convergence becomes unnecessary for convection to develop in the diagonal portion (Cocks 2003).

While these characteristics are well established, questions remain about temporal variations of the SPCZ and what implications such variations have for local and large-scale circulation patterns. It is also unclear why the SPCZ is spatially larger and contains more intense convection than other convergence zones, such as the South Indian Convergence Zone (SICZ; Cook 2000) and the South Atlantic Convergence Zone (SACZ) even though these zones are also oriented from the northwest to the southeast. Previous modeling studies have attempted to explain the unique intensity and location of the SPCZ with varied results. Yoshikane and Kimura (2003) suggest that convection is weakly related to surface temperature differences between Australia and the Pacific.

Kiladis et al. (1989) modeled the SPCZ by testing its sensitivity to the removal of Australia and South America in the model domain. Their findings suggest that the tropical (zonal) SPCZ is intensified by the West Australian Monsoon, while the removal of South America had little impact on the SPCZ. The subtropical and mid-latitude (diagonal) portion of the SPCZ remained insensitive to the continental configuration, further supporting the observational findings of its dependence on mid-latitude westerlies and dominant storm tracks.

The proximity of the tropical SPCZ to mesoscale convection over Indonesia suggests that the Madden-Julian Oscillation (MJO) (Madden and Julian 1994) could act as a possible mechanism for the formation of deep convection in the SPCZ. Matthews et al. (1996) describe how large convection regions north of Australia, triggered by the MJO, generate an upper-tropospheric anti-cyclone with subsequent increases in the wave structure of the subtropical jet stream. The study also explains that MJO events lead to an upper-level trough west of the SPCZ, making available ample baroclinic energy for the mid-latitude portion of the SPCZ.

Motivation for studying the variability of the Hadley and Walker circulations is driven in part by an effort to understand changes in the propagation of wave energy- both zonally and from the mid-latitudes into the tropics. Modeling (e.g., Webster and Holton 1982; Zhang and Webster 1989) and observational (e.g., Kiladis and Wheeler 1995) studies suggest that the strength of the westerly flow in the upper branch of the Pacific Walker cell has a strong influence on the ability for extratropical waves to propagate from the Northern Hemisphere (NH) into the equatorial region during December, January, and February (DJF). One of the major sources of variability in the upper

tropospheric westerly wind flow is changes in convection patterns throughout the SPCZ. The strength of the Hadley circulation also influences the propagation of waves from the tropical West Pacific, southeastward towards the mid-latitude South Pacific (Karoly 1989; Harangozo 2004). Composite analyses will be used in this study to address how anomalous patterns of convection alter the basin scale circulations.

We hypothesize that fluctuations in the spatial pattern of the SPCZ, ranging from synoptic to MJO timescales, cause pronounced changes in basin-scale circulation patterns over the Pacific. Changes in the structure of deep cumulus convection result in anomalous releases of latent energy from condensation processes (Liebmann and Smith 1996). The release of latent heat acts as an enhancing mechanism for the rising branches of the Pacific Hadley and Walker cells (Harangozo 2004). Increased convection may cause a magnitude change or spatial shift in the regional circulation patterns, depending on the location of anomalous rising air.

Variability of large-scale circulation patterns may also influence wave propagation within the SPCZ. For example, Cocks (2003) suggests that SH mid-latitude Rossby waves only interact with the tropical SPCZ when the zonal winds are sufficiently from the west, such as during and after MJO events. Webster and Chang (1988) demonstrate that wave group velocities approach zero in the tropics when westerly and easterly winds converge. We will explore how the accumulation of wave energy near the SPCZ is dependent on the mean flow, with increasing zonal accumulation occurring when the lower branch of the Walker circulation increases. Meridional wave energy accumulation is affected similarly by changes in the low-level flow of the regional Hadley circulation.

The data sets and methodology used in this study are presented in Chapter 2. We then present an overview of the climatology of the SPCZ, Hadley, and Walker circulations in Chapter 3. Important distinctions about the patterns of convection are made between the austral summer (DJF) and winter months of June, July and August (JJA). Chapter 4 explores the major dynamical processes involved in the mean state of the SPCZ with focus on the presence of strong boundary layer convergence, zonal accumulation of wave energy, and moderate cross-equatorial wind bursts. This climatology will be related to observing how the SPCZ varies on sub-monthly to MJO timescales (Chapter 5) and the associated changes in teleconnection processes (Chapter 6).

Chapter 7 synthesizes the key findings of how dynamical processes govern SPCZ variability and cause interactions with large-scale circulation patterns. Consequences of the association between anomalous convection and regional Hadley and Walker circulation changes for wave energy propagation are explored. Additionally, this chapter contains important avenues for future research including how anomalies in the meridional flow impact the SPCZ. Plans are also discussed for looking at whether mid-latitude waves transfer signals between developing MJO convection and the South Pacific. We explore last how long-term climate trends may alter convection patterns and lead to changes in the magnitude of the Walker circulation.

CHAPTER 2

DATA AND METHODS

This chapter provides a detailed discussion of the data sets and methods of analysis used to describe the climatology of the South Pacific region (20˚N-40˚S, 120˚E-290˚E) and associated large-scale circulation patterns. Explanations are also given for how the dominant modes of variability are extracted from the data and used to create composite anomalies.

2.1 Observational Data Sets

The tropical atmosphere and oceans are diagnosed using satellite derived measurements in addition to model reanalysis data. National Oceanic and Atmospheric Administration (NOAA) Optimum Interpolation (OI) data from the Climate Diagnostics Center (CDC) are used in this analysis to characterize underlying sea surface temperatures (SSTs) in the SPCZ. These observations extend from December 1981 to August 2006 with a spatial resolution of 1˚ Latitude by 1˚ Longitude (Kistler et al. 2001). The dataset is interpolated spatially and averaged monthly to minimize the impact of poor data caused by satellite orbital characteristics or meteorological interference.

Outgoing longwave radiation (OLR) satellite measurements are used as a proxy for atmospheric moist convection. NOAA OLR data extending from December 1981 to August 2006, interpolated onto a 2.5˚ by 2.5˚ spatial grid (Liebmann and Smith 1996), are used to calculate daily mean OLR measurements. Sources of error include the occasional development and dissipation of storms in between twice daily observations and large cirrus clouds, with similar temperature to cumulonimbus cloud tops, which

blow away from deep convection further distorting the data (by up to 12 hours). Despite sources of possible error, OLR has been used in many previous studies to analyze tropical waves, the ITCZ, and the SPCZ (e.g., Wheeler and Kiladis 1999; Wheeler and Weickmann 2001; Gu and Zhang 2002). Extensive cirrus cover of non-convective origin is also frequently observed near subtropical jet streams (Schnadt et al. 1997) and must be considered as a possible source of error when using OLR to infer convection outside of the tropics.

The final dataset used in this analysis comes from the National Centers for Environmental Prediction / National Center for Atmospheric Research (NCEP/NCAR) reanalysis dataset (Kalnay et al. 1996). The reanalysis project describes the global atmosphere through the assimilation of satellite, ground, ship, and balloon based observations as well as output from computer models to infer variables in regions for which reliable observations are unavailable. Variables are separated into three types based on the methods used to obtain them. Type A variables are those directly measured including surface temperature and pressure as well as atmospheric profiles from weather balloons or satellites. Detection systems are often not extensive enough to measure the atmosphere at the desired spatial (2.5˚x2.5˚, 17 pressure levels) and temporal (four times daily) frequencies. In this case, a combination of observations and computer modeling is used to produce Type B variables. Type C variables are derived completely from modeling algorithms and are therefore subject to the largest error sources due to problems with the original observations, modeling resolution, or parameterization schemes. For example, precipitation is a Type C reanalysis variable which has proved particularly prone to error in the tropics because of problems with the convective parameterization

scheme used in the NCEP/NCAR reanalysis. This is apparent in the SPCZ, where the reanalysis precipitation field, oriented parallel to the equator, shows little resemblance to the characteristic diagonal pattern of the convergence zone (Cocks 2003). We do not use Type C reanalysis data sources in this study and instead infer precipitation patterns from satellite measurements of OLR.

Reanalysis wind and mean sea-level pressure (SLP) variables are utilized in this study. Divergence (δ) and relative vorticity (ζ) are derived from the zonal and meridional wind data (*u* and *v*) to aid in the dynamical description of the SPCZ using Equations 1 and 2, respectively.

$$\delta = \left(\frac{\partial u}{\partial x} + \frac{\partial v}{\partial y} \right) \tag{1}$$

$$\zeta = \left(\frac{\partial v}{\partial x} - \frac{\partial u}{\partial y} \right) \tag{2}$$

From here, the divergent component of the mean wind field can be extracted for analysis of cross-equatorial flows in Chapter 4. We also separate the zonal and meridional components of δ to analyze the stretching deformation terms $\frac{\partial u}{\partial x}$ and $\frac{\partial v}{\partial y}$, respectively. Absolute vorticity $(\eta = \zeta + f)$ is further diagnosed as the sum of the Coriolis parameter (*f*) and the ζ field. Special attention is given in Chapter 4 to departures of the zero absolute vorticity contour away from the equator as an indication of cross-equatorial flow.

Mass stream functions are also calculated from the zonal (Equation 3) and meridional (Equation 4) reanalysis winds:

$$\psi_Z = \frac{a}{g} \int_{10^\circ S}^{10^\circ N} \int_0^P u^* \, dp \, d\phi \tag{3}$$

$$\psi_M = \frac{2\pi a \cos\phi}{g} \int_0^p [v] \, dp \tag{4}$$

where a is the mean radius of the earth, g is the acceleration of gravity, φ is latitude, and p is atmospheric pressure (Hartmann 1994). The horizontal (vertical) gradient of the zonal stream function (ψ_Z) is representative of the rising and subsiding (upper and lower) branches of the Walker circulation. Gradients of the meridional stream function (ψ_M) are used in a similar manner to measure the strength of the Hadley circulation averaged over longitudinal ranges corresponding to the Central and West Pacific regions.

2.2 Statistical Methods

The climatology section (Chapter 3) presents seasonal averages for austral summer and winter SST, SLP, OLR, divergence at the 925 and 200 hPa levels, and averages of the Hadley and Walker circulations. Dynamical processes involved in the SPCZ (Chapter 4) are diagnosed using seasonal averages of zonal and divergent winds, as well as cross sections of divergence (δ) and stretching deformation ($\frac{\partial u}{\partial x}$ and $\frac{\partial v}{\partial y}$). Composite analysis methods, similar to those employed by Fukutomi and Yasunari (2005) are used to measure the response of convection in the SPCZ to cross-equatorial wind bursts.

Principal modes of SPCZ convective variability are first distinguished using Fourier power spectra of OLR in Chapter 5 (e.g., Hartmann 2005). Wavelet analysis techniques (Torrence and Compo 1998; Cromwell 2001; Grinsted, Moore, and Jevrejeva 2004) are further used to determine when, and in which portions of the SPCZ, major modes of variability occur (Chapter 5). Wavelet coherence analysis (Grinsted, Moore, and Jevrejeva 2004) between the tropical, subtropical, and mid-latitude regions of the SPCZ show significant spatial interactions during a case study of a MJO event propagating across the West Pacific.

Bandpass filters of daily OLR are used to extract particular modes of variability to construct composites of sub-monthly cross-equatorial surges (Chapter 4.2) and MJO

events (Chapter 5.2). We have chosen to use a Lanczos filter (Duchon 1979) with 249 weights for the 6-25 day filter (Fukutomi and Yasunari 2005) and to extract MJO signal between 25-80 days. Normal filtering rules apply with increased number of weights resulting in improved results, but also more data loss at each end of the time series. We have chosen to use 249 weights for each bandpass filter to remain consistent with earlier studies. Our time series are sufficiently long (1982-2006) that loss of several months of data at either end does not cause distortions to the results. Empirical Orthogonal Function (EOF) analysis of the 25-80 day filtered OLR shows a clear spatial and temporal signal of the MJO propagating from the Indian Ocean into the SPCZ (Matthews 2000). Descriptions of EOF analysis can be found in Wilks (1995) and Hannachi (2004). Lead/lag composites of OLR, zonal wind, and mass flux daily anomalies are produced using dates from the Principal Components (PCs) of the EOF analysis. These composites show how MJO events increase storm activity in the SPCZ (Chapter 5.2) and what impacts this has on the regional Hadley and Walker circulations (Chapter 6.2).

Statistical significance, at the 95% level, is assessed using the Student's t test for composite analyses, whereas the 95% confidence intervals, for spectra and wavelets, are based on the lag-1 autocorrelations (red noise spectrum) of the time series (Torrence and Compo 1998). Monte Carlo methods utilizing 300 random trials are used to compare the wavelet coherence results against a red-noise process (Grinsted, Moore, and Jevrejeva 2004). These significance levels are displayed using solid black contours and will be discussed in more detail throughout the later chapters.

CHAPTER 3

CLIMATOLOGY

To gain an understanding of the spatial extent of the SPCZ, we first compile a comprehensive climatology which presents the basic state (SST and SLP) and differentiates between the tropical (zonal) and mid-latitude (diagonal) components, using OLR and divergence maps. We begin by creating austral summer and winter averages of these variables because maximum and minimum intensity of the SPCZ occurs during summer and winter, respectively. Throughout this section of the paper, plots extend from 20˚N to 40˚S and from 120˚E to 290˚E. This mapping allows us to compare the SPCZ with other regions of South Pacific Basin. Seasonal mean plots of the regional Hadley and Walker circulations are also presented here. We show additionally how the Pacific Walker cell varies over time and propose some mechanisms for how the SPCZ may influence the general atmospheric circulation.

3.1 South Pacific Convergence Zone

Seasonal plots of SSTs show that the large expanse of the West Pacific Warm Pool (defined as the region of the Pacific Ocean where SSTs are greater than 29˚C) reaches furthest south during austral summer (Figure 3.1a). In the austral winter (Figure 3.1b), the warmest waters are located north in the Philippine Sea. The SLP field shows a similar seasonal oscillation (Figure 3.2). Mean pressures lower than 1010 hPa are mostly found over the West Pacific Warm Pool. Cooler SSTs in the Southeast Pacific form a dominant high pressure region near the surface. Northwesterly flow around the lower pressure converges with the northeasterly circulation from the high, producing an extensive convergence zone. Near surface specific humidity (q_{925hPa}) also correlates

strongly with the location of warmest SSTs. We will demonstrate later that deep convection associated with the tropical portion of the SPCZ closely follows the seasonal SST, SLP, and surface moisture content cycles. Not shown in Figure 3.1 are the warm waters in the Eastern Indian Ocean which underlie the formation region of MJO convection bursts that will be shown to interact quite often with the SPCZ during austral summer. It is evident from meridional SST gradients displayed in Figures 3.1c and 3.1d that a sharp dividing line exists between the West Pacific Warm Pool and much cooler waters of the Southern Ocean. Further analysis will be given in the next chapter on the role of the sharp temperature gradient in providing baroclinic energy to the subtropical and mid-latitude portions of the SPCZ.

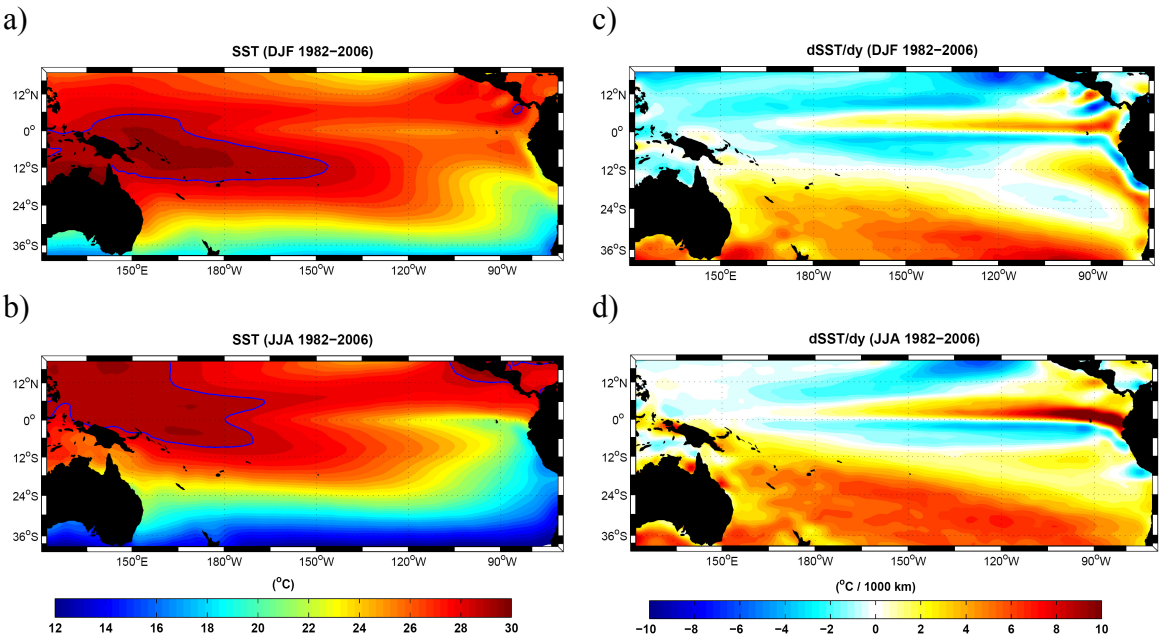

Figure 3.1 Seasonal averages of SST (˚C) during austral summer (a) and winter (b). The 29˚C isotherm is outlined by a thin blue line. Corresponding meridional SST gradients (˚C/1000 km) for austral summer and winter (c and d).

a)

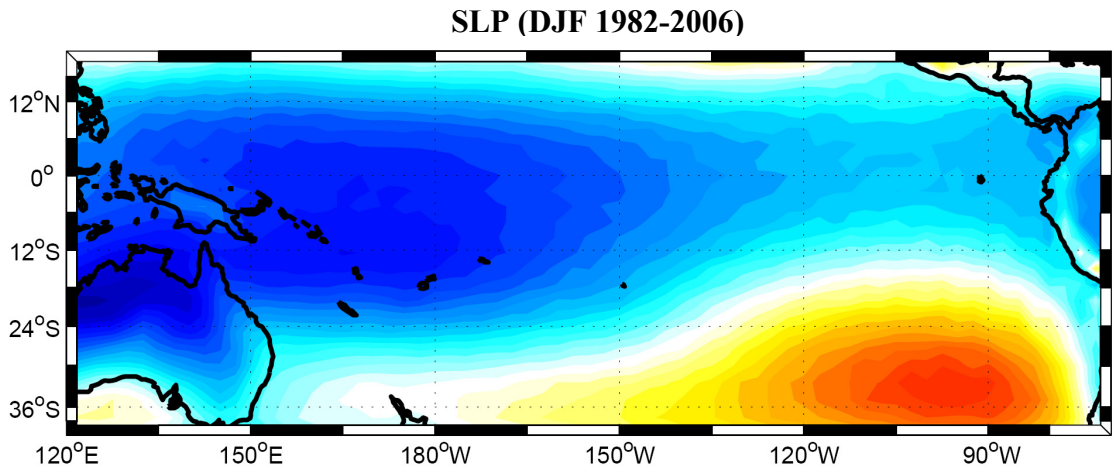

b)

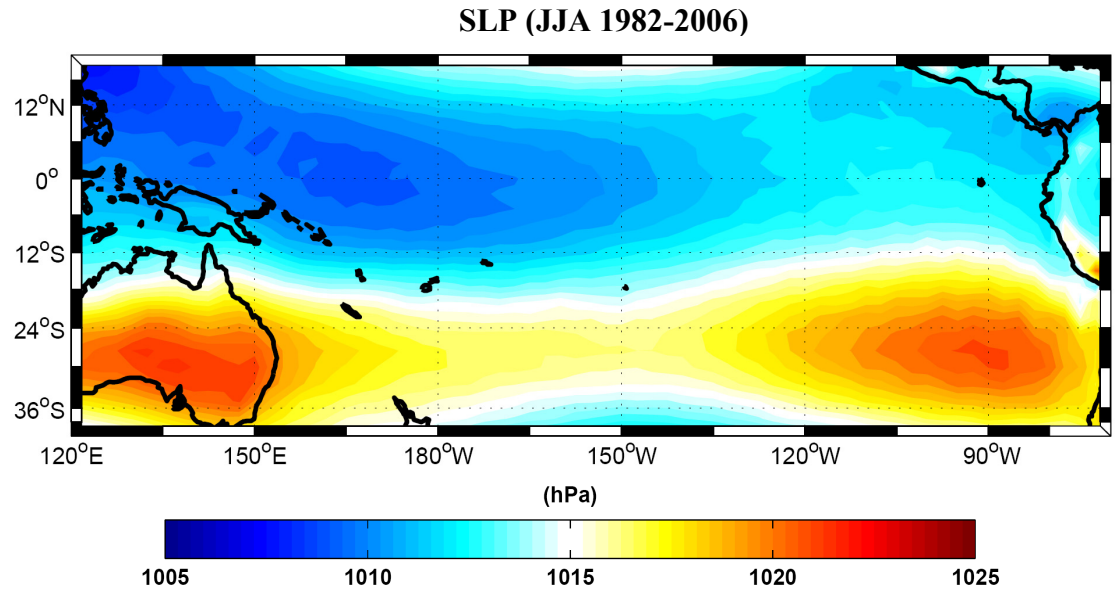

Figure 3.2 Seasonal averages of SLP (hPa) during austral summer (a) and winter (b).

The seasonal nature of the SPCZ becomes increasingly clear by looking at the OLR field. A narrow strip of low OLR, as evident by the cooler colors, is associated with convection of the ITCZ which extends zonally around the equator during DJF (Figure 3.3a) and JJA (Figure 3.3b). Convection expands meridionally over the West Pacific Warm Pool and Indian Ocean. During austral summer (Figure 3.3a), OLR minima extend away from the West Pacific ITCZ in a southeastward direction towards the SH mid-latitudes. This extension corresponds to the largest spatial extent and maximum intensity of convection along the SPCZ. By austral winter, most of the convection has shifted towards the north, following the annular progression of the Warm Pool. The deepest convective regions (OLR less than 230 Wm^{-2}) are outlined by a red line for visual clarity. Hence, the maximum (minimum) deep convection in the SPCZ occurs during DJF (JJA). For this reason, in the next chapter we limit our analysis of the dynamical processes to these two seasons. Previous studies (e.g., Vincent 1994; Karoly and Vincent 1999) show that strong vertical ascent in the troposphere is found in the same regions with OLR values less than 230 Wm^{-2}. Rising air, omega ($\omega<0$), is often measured at the 500 or 400 hPa level where vertical lift in convection is typically the most intense. Maps of 400 hPa ω show vigorous ascent (approaching 90 hPa day^{-1}) throughout the tropical, subtropical, and mid-latitude SPCZ during austral summer. However, winter OLR (Figure 3.3b) shows that the subtropical SPCZ is void of persistent convective cloud cover, with the tropical and mid-latitude longitudinal extents narrowing. Karoly and Vincent's (1999) analysis of winter ω shows similar reduced convection along the SPCZ compared to the summer with a region of subsidence ($\omega>0$) in the subtropics.

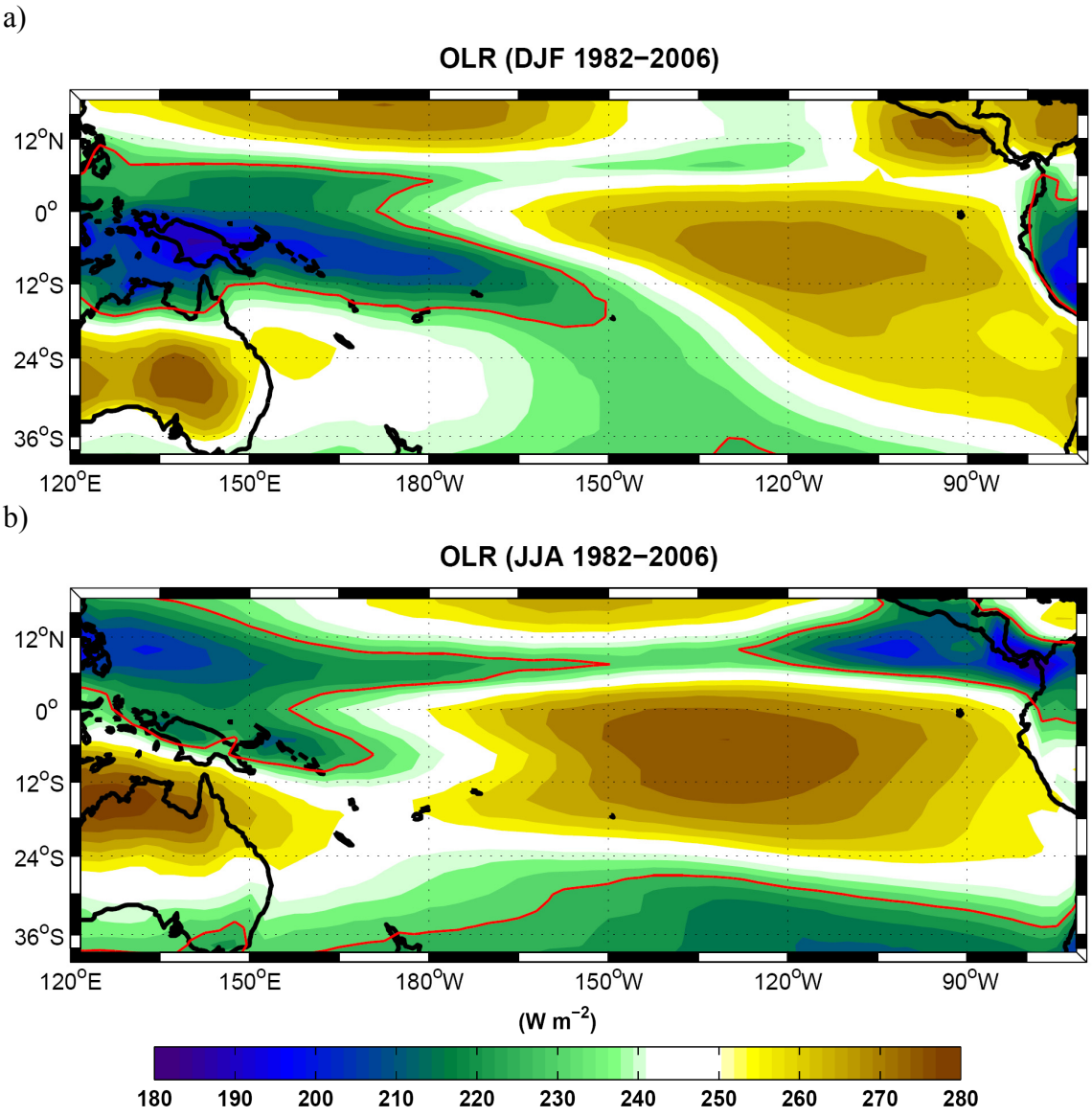

Figure 3.3 Seasonal averages of OLR (Wm^{-2}) during austral summer (a) and winter (b). The 230 W m^{-2} contour is outlined by a thin red line.

Robust evidence of seasonal changes in the SPCZ are evident in the divergence fields (δ) at the 925 and 200 hPa levels during austral summer and winter (Figure 3.4). Strong convergence $(\delta < 0)$ at the 925 hPa level is present throughout the ITCZ and SPCZ during the summer months. During winter, the ITCZ and associated convergence migrates north, while a divergent environment is found in the SPCZ poleward of 15˚S. At higher levels (e.g., 850 hPa, not shown), we find a convergent pattern along the austral summer SPCZ that is more diagonal and separated from the Central Pacific ITCZ. The convergence pattern above the boundary layer is more similar to the OLR signature, especially in the tropical (zonal) region. Further southeast, the boundary layer convergence pattern (925 hPa) becomes increasingly diagonal and is associated with the precipitation pattern as suggested by the DJF OLR. In austral winter (Figure 3.4c), we see that there is a divergent pattern throughout the subtropics at the 925 hPa level. This divergence region divides the convergence over the West Pacific Warm Pool and mid-latitude storm tracks situated to the south.

Previous studies of the relationship between local SSTs and divergence patterns have produced varied results. Kiladis et al. (1989) show that the maximum surface convergence of the SPCZ is found poleward of the warmest SSTs and is perhaps a result of the strong SST gradient. By contrast, Cocks (2003) suggests that the maximum convergence is shifted more equatorward. Our analysis suggests that there is a slight, seasonally dependent, spatial departure between maximum convergence and ocean temperatures. During austral summer, maximum convergence at 925 hPa is found in a more diagonal pattern, and therefore displaced poleward of the warmest waters. The opposite arrangement occurs during austral winter when the convergence pattern at this

level becomes more zonally oriented and centered along the equator. Physical mechanisms which explain these patterns will be explored in Chapter 4.

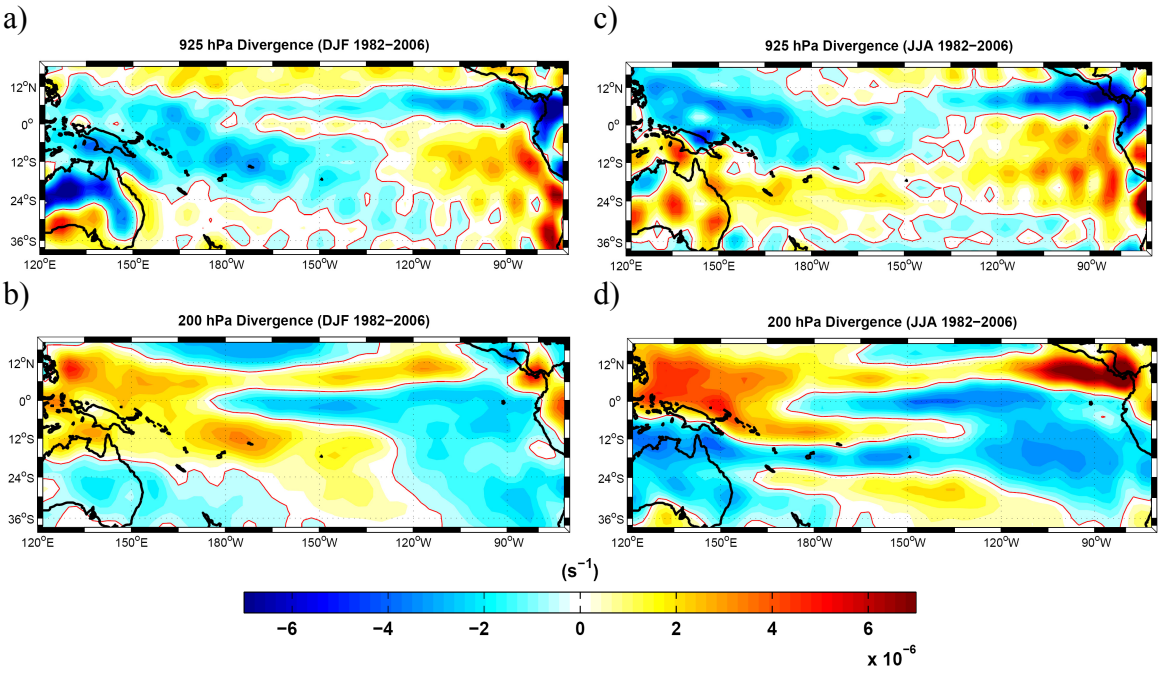

Figure 3.4 Plots of divergence during austral summer (winter) at the 925hPa (a) and 200hPa (b) levels (winter: c and d). The zero contour is indicated by the thin red line. Cooler (warmer) colors represent convergence (divergence).

Upper tropospheric (200 hPa) divergence (Figures 3.4b and d) reveals ridging patterns in regions with boundary layer convergence and deep convection (OLR < 230 Wm^{-2}). The zero divergence contour (red lines in Figure 3.4) clearly outline major precipitation regions in the ITCZ and SPCZ during austral summer. Perhaps the most

striking seasonal distinction is the region of strong upper level convergence separating the tropical and mid-latitude sections of the SPCZ during austral winter (Figure 3.4d). The separated pattern of 200 hPa divergence provides further credence to the observation that subsidence divides the winter SPCZ. In the next section, we will discuss how this region of subsidence influences the Hadley circulation over the Southwest Pacific.

It is important first to characterize how the ITCZ interacts dynamically with the SPCZ. We have discussed convection in the Pacific ITCZ merging with the SPCZ over the Indonesian region during summer and winter (OLR, Figure 3.3). These plots are derived using seasonal means from 1982-2006 and should not be considered an indication that the ITCZ and SPCZ are always merged together. An index of the relative strength of the tropical SPCZ compared to the ITCZ is adapted from Harangozo (2004) for the austral summer and winter seasons (Figure 3.5a, black and dashed-blue lines, respectively). The index is determined by subtracting the seasonal average of OLR within the SPCZ from that associated with the ITCZ. In order to capture regions of deepest convection, these averages are calculated over the (10˚S-15˚S, 190˚E-200˚E) and (5˚N-10˚N, 150˚E-160˚E) spatial grids for the DJF SPCZ and ITCZ, respectively. These grid choices are substantiated by the EOF analysis (Figure 3.5b) which shows maximum coupled variance between these two regions. During JJA, we use a spatial grid of (2.5˚S-5˚S, 165˚E-175˚E) and (0˚N-2.5˚N, 165˚E-175˚E) for the SPCZ and ITCZ, respectively. In this case, the grids share the same longitude range because the eastward extent of the SPCZ is greatly diminished during JJA. Positive (negative) index values indicate that the largest expanse of low OLR, associated with the deepest convection, is located in the

SPCZ (ITCZ). This sign convention has been picked for convenience when focusing on the SPCZ and is opposite of that used by Harangozo (2004).

An alternate method for diagnosing spatial variations of convection patterns is to perform an EOF analysis of OLR data. Here we will first apply a 6-25 day bandpass filter to daily anomalies of OLR to avoid longer period variability. Figure 3.5b shows a clear "seesaw" pattern of convection over the West Pacific. The EOF analysis confirms that there is a connection between anomalous convection over the northeastern SPCZ during periods when the ITCZ over the West Pacific Warm Pool is experiencing positive OLR anomalies of 10-20 Wm^{-2}. Additionally, convection in the southwest SPCZ decreases when the ITCZ is weak. The reverse association with above normal ITCZ convection, during periods of minimal northeastern SPCZ storms, also holds. A caveat of the EOF analysis is that the first PC only explains about 4.2% of DJF sub-monthly OLR variability. It does suggest, however, a possible relationship between convection in each hemisphere of the West Pacific. Possible dynamical explanations for cross-equatorial interactions will be discussed in Chapter 4.2.

On longer time scales, we infer from Figure 3.5a that the amount of ITCZ and SPCZ interaction varies greatly between summer and winter and from year to year. In general, the SPCZ is stronger and separate from the ITCZ during most austral summers and many winters, as evident by the frequency of positive index values. When the index is close to zero, it suggests a high degree of interaction between the ITCZ and SPCZ, even during the summer (e.g., 1986, 1993, 1997, 2001, and 2002). Negative values in winter are caused by the increased relative strength of the ITCZ as convection migrates north following the West Pacific Warm Pool.

a)

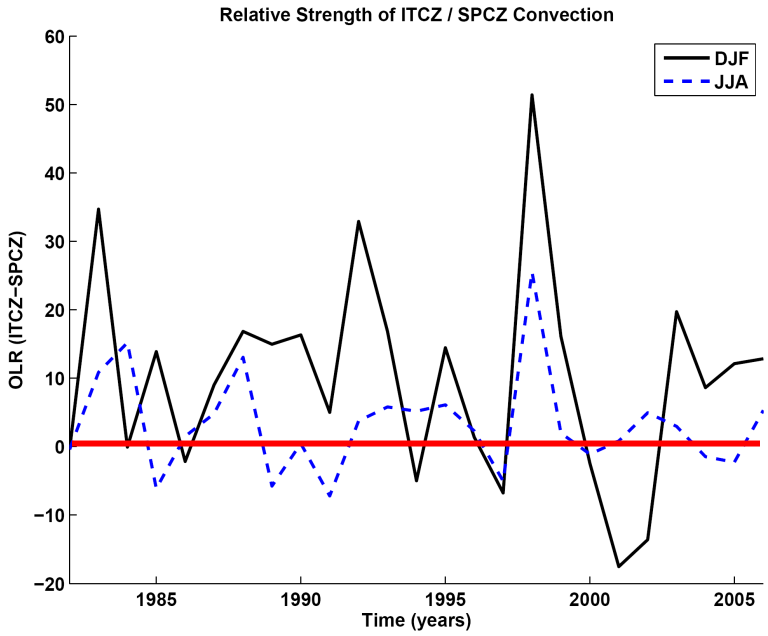

b)

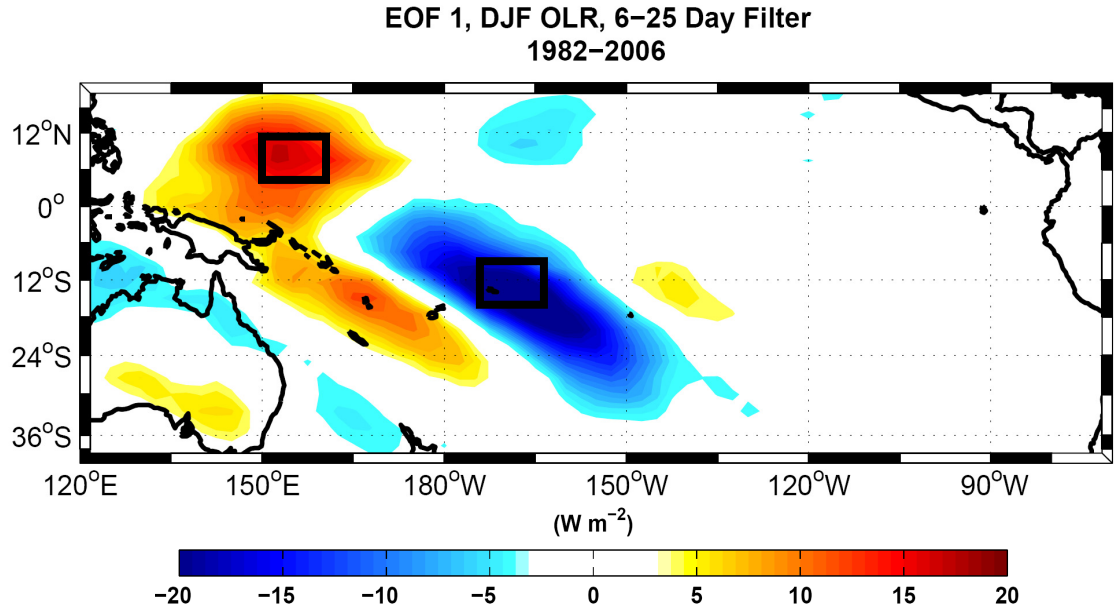

Figure 3.5 Index of the relative amounts of convection in the SPCZ and ITCZ (a). Spatial grid of the DJF SPCZ and ITCZ is (10˚S-15˚S, 190˚E-200˚E) and (5˚N-10˚N, 150˚E-160˚E), respectively. Spatial grid of the JJA SPCZ and ITCZ is (2.5˚S-5˚S, 165˚E-175˚E) and (0˚N-2.5˚N, 165˚E-175˚E), respectively. Positive (negative) indices indicate that the SPCZ (ITCZ) is stronger. First EOF of 6-25 day bandpass filtered DJF OLR (b). Black squares represent the SPCZ (lower) and ITCZ (upper) grids used to compile the DJF index (a).

3.2 Hadley Circulation

The Hadley circulation is depicted typically as a meridional cell of rising air near the equator, which flows poleward in the upper levels of the troposphere, before sinking back towards the surface in the subtropics. Meridional winds near the surface then return air back towards the equatorial region. The thermally direct nature of the circulation typically results in the rising branch being collocated with the warmest surface temperatures, usually just poleward of the equator in the summer hemisphere (Hartmann 1994). A diagnostic relationship for the vertical velocity (ω) within the troposphere is produced by scaling the Thermodynamic Energy Equation (Equation 5) for synoptic-scale motions in the tropics (Equation 6) (Holton 2004):

$$\left(\frac{\partial}{\partial t} + V \bullet \nabla\right) T + \frac{\omega N^2 H}{R} = \frac{J}{C_P} \tag{5}$$

$$\frac{\omega N^2 H}{R} = \frac{J}{C_P} \tag{6}$$

where N is the buoyancy frequency, H is the scale height, R is the gas constant for dry air, J is the diabatic heating rate, and C_p is the specific heat at constant pressure. The transition from Equation 5 to 6 is achieved because synoptic-scale temperature advection is negligible in the tropics. The diabatic cooling of the troposphere through emission of longwave radiation $\left(J/C_P \approx 1 K day^{-1}\right)$ must therefore be balanced by adiabatic warming due to slow subsidence.

In reality, strong cumulous convection releases latent heat into the tropical atmosphere by condensation processes. The average heating rate per unit mass of air therefore increases by about five times $\left(J/C_P \approx 5 K day^{-1}\right)$ (Holton 2004). Equation 6 suggests that there would be vigorous ascent in regions of cumulous convection (low OLR values) surrounded by larger regions of slowly subsiding motions. This clearly

suggests that the location of deep convection has a strong impact on the placement of the rising and subsiding branches of the Hadley circulation.

Meridional cross sections of mass stream functions are shown for three longitudinal subsections (150°E-180°E, 180°E-210°E, 210°E-240°E) of the Central and Western South Pacific during austral summer and winter (Figure 3.6). During summer, vigorous ascent is concentrated between 10°S-30°S while the equatorial region is generally subsident. In order to achieve conservation of mass, the horizontal flow must be from equator to pole in the low levels and reversed in the upper troposphere. These circulation patterns are in opposition to the global mean meridional circulation with the strongest vertical ascent above the warmest surface temperatures near the equator. Additionally, these "reversed" Hadley cells appear to shift poleward as we move from west to east along the summer SPCZ. Locations of the rising branches closely match the diagonal orientation of deep convection observed by the OLR minima in Figure 3.3.

During austral winter, SPCZ convection shifts equatorward into the Indonesian region, where we observe an enhancement of the NH ITCZ. Vertical ascent occurs near the equator in western subsection (150°E-180°E) and is collocated with the tropical portion of the winter SPCZ. Further east, rising motions are shifted northward to around 10°N and correspond with the mean location of the ITCZ. There is also moderate ascent occurring between 20°S-30°S in the eastern subsections (Figure 3.6e and f) which is collocated with the dominant tracks of mid-latitude storm systems. These observations suggest that strength and location of the SPCZ, as well as its relative intensity compared to the ITCZ, impact the regional Hadley circulation.

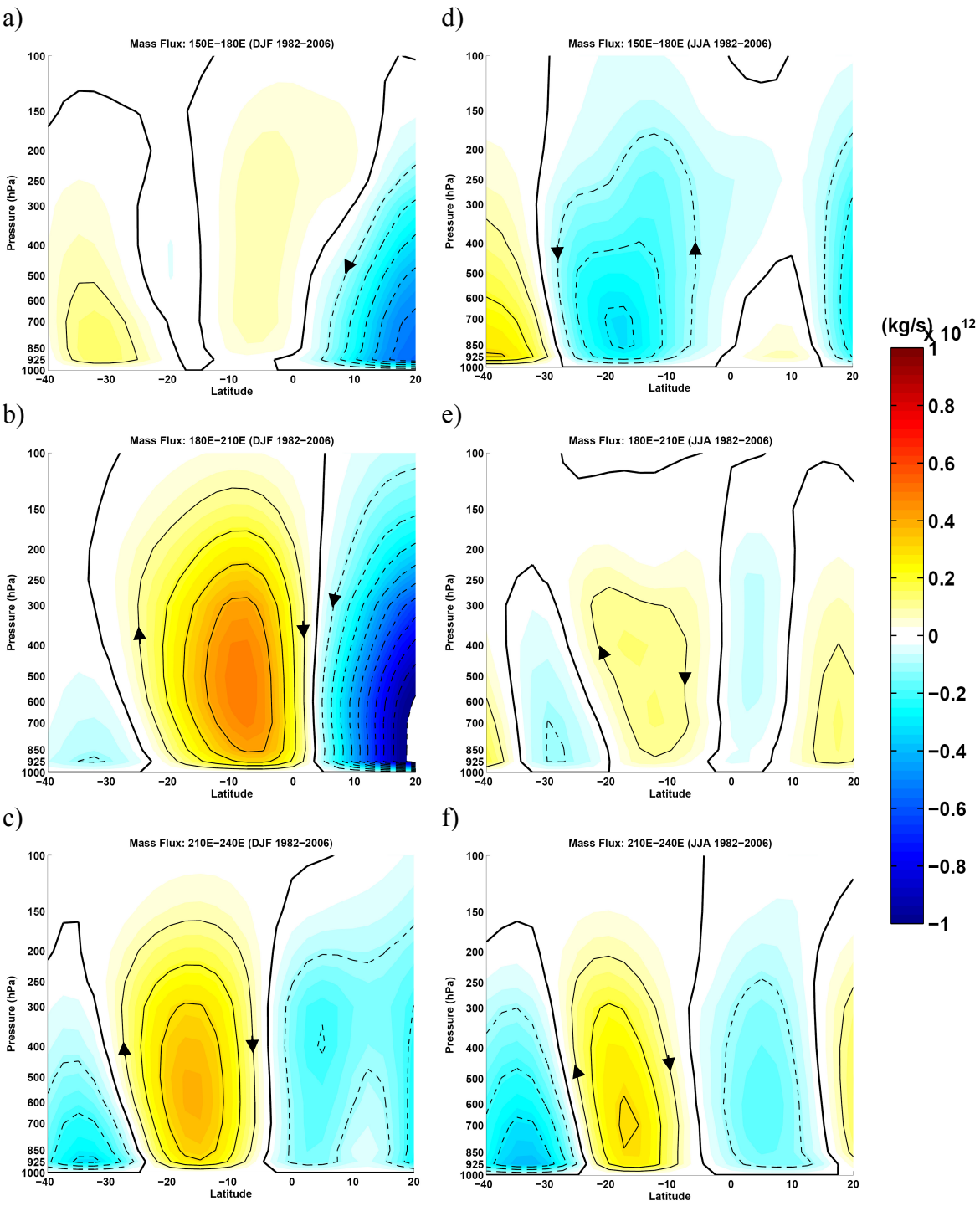

Figure 3.6 Meridional cross sections of mass stream functions. Austral summer (winter) averages displayed in subplots a) 150˚E-180˚E, b) 180˚E-210˚E, and c) 210˚E-240˚E (winter: d, e, f). Zero contour indicated by the thick black line. Contour interval is 10^{11} kg/s (solid: positive, dashed: negative, and arrows indicate direction).

3.3 Walker Circulation

The strength of the mean Pacific Walker circulation (e.g., $5x10^{10}$ kg/s during DJF) is an order of magnitude smaller than the meridional cells (e.g., $4x10^{11}$ kg/s) we discussed in the previous section. We use zonal cross sections of mass stream functions averaged from 10°N-10°S to depict the summer and winter Pacific Walker cell (Figure 3.7a and c, respectively). While the longitudinal range of the cross sections are global, our focus is on the Pacific Basin (120°E-290°E). Flow is again clockwise, in the longitude-pressure plane, around positive stream functions with the circulation magnitude being directly proportional to the mass flux gradient. Regions of vertical ascent are correlated with the location of the West Pacific Warm Pool and associated deep convection. Subsidence typically occurs over the cooler waters of the Central and Eastern Pacific. There is also vigorous ascent around 300°E associated with convection over the Amazon Basin.

During austral summer, the relative strength of the Walker circulation is almost five times stronger than the winter circulation. Stronger (weaker) vertical wind shear also occurs over the Central Pacific (220°E-240°E) when the circulation is more (less) intense (Figure 3.7b and d, respectively). The index of vertical wind shear can therefore be used as an alternate measure of the zonal circulation. From the time series of wind shear from 1982-2006, we observe a high degree of daily variability as well as interannual fluctuations (austral summer, b). Minima in seasonal mean vertical wind shear typically occur during El Niño events (e.g., 1987, 1992, and 1997). These El Niño events are associated with a warming of the East Pacific and a subsequent eastward shift of equatorial storminess and deep convection (Trenberth 1997). It is reasonable to assume that this eastward shift of warm SSTs and convection causes a decrease in the Pacific Walker circulation and vertical wind shear over the Central Pacific.

The seasonal mean OLR plots in Figure 3.3 suggests that convection is also oriented substantially further east during JJA compared with DJF. The more evenly

distributed convection along the equator during austral winter forces a much weaker zonal circulation. It will be shown in Chapter 4 that the lower branch of the Walker circulation (easterly trade winds) is one of the major components necessary for the accumulation of wave energy near the SPCZ. We hypothesize therefore that a weaker climatological winter circulation results in less dynamical support of deep convection in the SPCZ. We also pose a pair of questions concerning how SPCZ convective fluctuations influence the Hadley and Walker circulations, and what impact this may have on regional wave propagation. These questions will be investigated in Chapter 6 using composites of the Hadley and Walker cells based on times of maximum SPCZ convection.

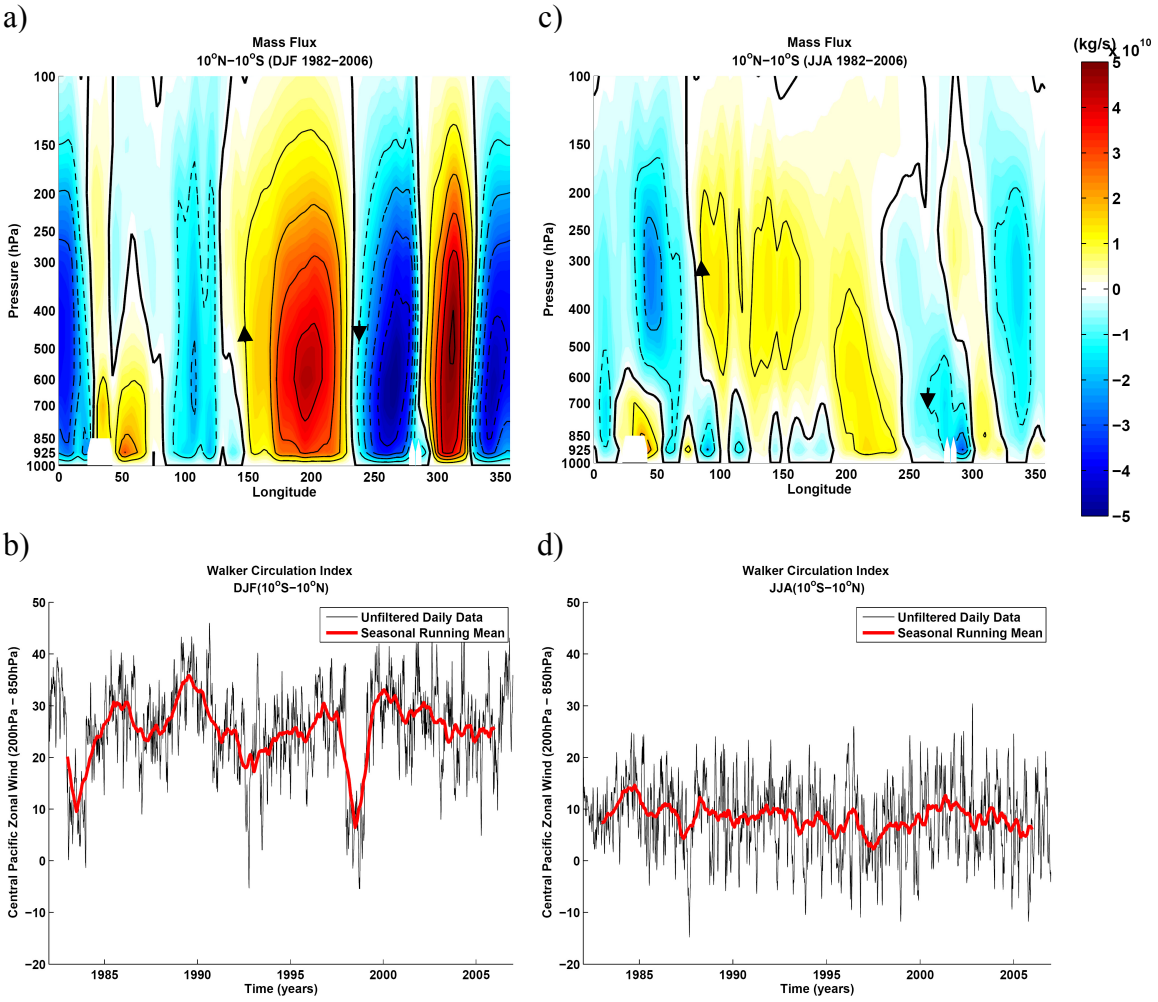

Figure 3.7 Zonal cross sections of mass stream functions averaged from 10˚N-10˚S for austral summer (a) and winter (c). Zero contour indicated by the thick black line. Contour interval is 10^{10} kg/s (solid: positive, dashed: negative, and arrows indicate direction). Time series of the vertical wind shear averaged over the Central Pacific (220˚E-240˚E) during summer (b) and winter (c). Seasonal running mean indicated by the solid red lines.

CHAPTER 4

DYNAMICAL PROCESSES

Climatological plots show that the SPCZ is divided into two types of convergence zones. In the tropical latitudes, storminess is typically co-located with the zonal SST maximum (Cocks 2003), whereas mid-latitude cyclonic weather systems drive instability further south in the diagonal part of the convergence zone. We will now explore the dynamical explanations for the spatial arrangement of the SPCZ and why the pattern changes on seasonal timescales. Some studies suggest that strong boundary layer convergence fuels cumulonimbus development in the tropical and subtropical regions (e.g., Hurrell and Vincent 1987; Kiladis et al. 1989; Vincent 1994; Yoshikane and Kimura 2003). Further south, the subtropical jet stream emerges from the Australian coast, producing strong vertical wind shear. Additional instability may be provided by moderate cross-equatorial flow (Tomas and Webster 1997; Tomas et al. 1999) and wave energy accumulation (Webster and Chang 1988). This latter source is expected to amplify storm development throughout all latitudes of the SPCZ.

4.1 Vertical Wind Shear

Warm SSTs (> 27.5˚C) during DJF (Figure 3.1a) and abundant low-level moisture, indicated by high specific humidity ($q_{925\ hPa}$ > .013 kg/kg), provide the thermodynamic support for deep convection in the tropical SPCZ (e.g., Graham and Barnett 1987). Several studies have proposed that the subtropical and mid-latitude SPCZ are enhanced by a baroclinic atmosphere due to a stronger meridional gradient in SST (Hurrell and Vincent 1987; Kiladis et al. 1989; Karoly and Vincent 1999). The strong

meridional SST gradient throughout these regions during austral summer (Figure 3.1c) begins to encroach on the tropical latitudes in winter (Figure 3.1d), when the warm pool recedes north and the East Australian northerly ocean current weakens (Karoly and Vincent 1999).

A westerly jet maximum at the 200 hPa level emerges off the East Australian coast and closely follows the meridional surface temperature gradient into the diagonal portion of the SPCZ. This jet stream reaches its highest magnitude during winter when the temperature gradient is also greatest, consistent with the thermal wind balance relationship. Assuming geostrophic processes, we see that the zonal wind (u_g) is related to the atmospheric thickness gradient by Equation 7 (Holton 2004).

$$u_g = -\frac{1}{f}\frac{\partial \Phi}{\partial y} \tag{7}$$

Where the meridional thickness gradient, $\left(\frac{\partial \Phi}{\partial y}\right)$, points from the equator towards the mid-latitudes due to the sharp SST gradient and f is the Coriolis parameter.

Vertical wind shear creates a baroclinic environment which supports the development of mid-latitude cyclonic weather systems and amplifies the mid-latitude (austral summer and winter), as well as subtropical (austral winter), portions of the SPCZ. Looking at meridional cross sections of zonal wind (Figure 4.1), we observe vertical wind shear $\left(\frac{\partial u}{\partial z}\right)$ throughout the mid-latitudes and subtropics. This is due to the large difference between the westerly jet, centered at 200 hPa, and the more easterly winds near the surface. This vertical wind shear becomes stronger during winter (stronger SST

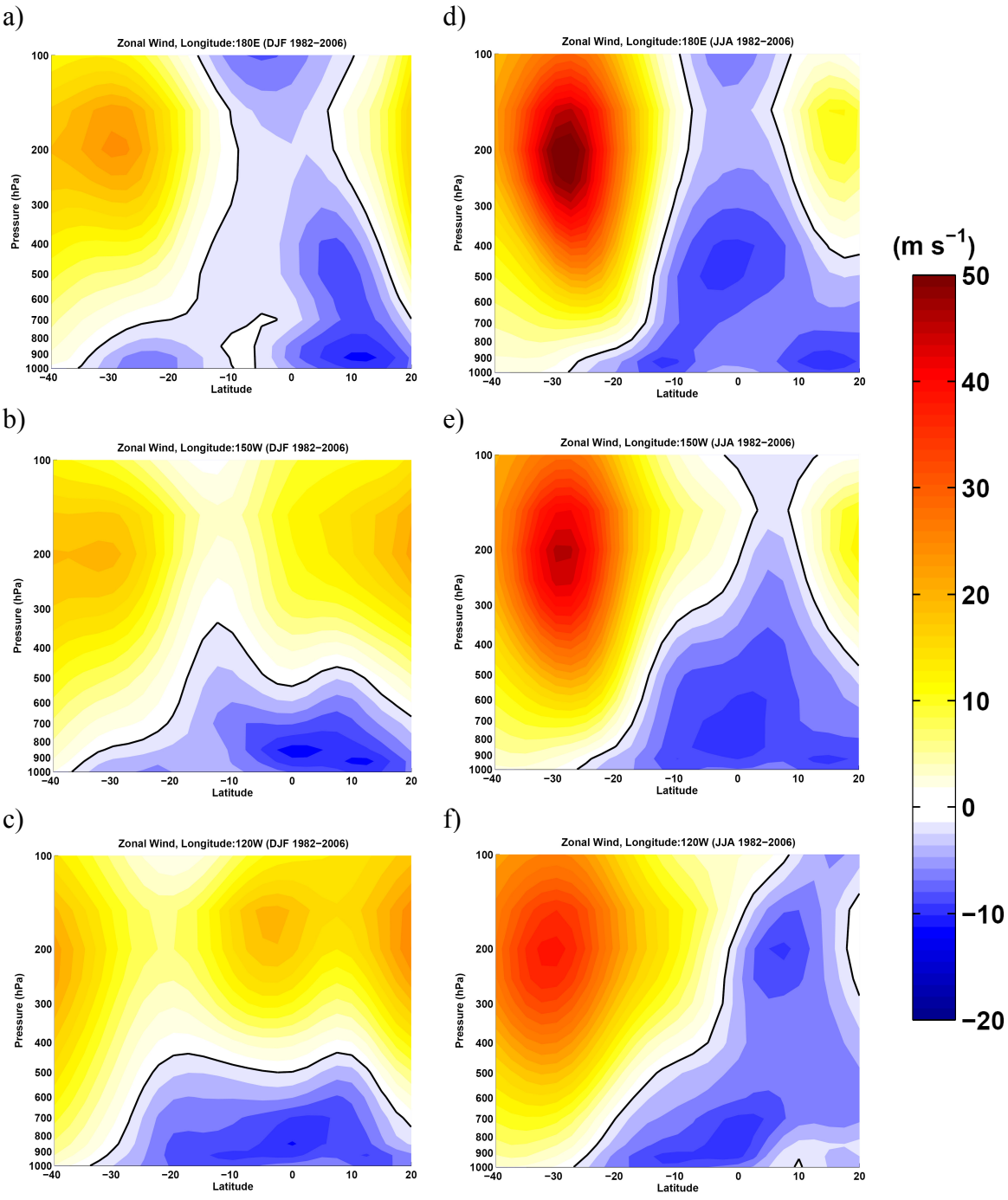

Figure 4.1 Meridional cross sections of zonal winds. Austral summer (winter) averages displayed in subplots a) 180˚E, b) 150˚W, and c) 120˚W (winter: d, e, f). Zero contour indicated by the solid black line.

gradient) and extends further towards the equator. The equatorial progression of the jet maximum follows the seasonal migration of the greatest SST gradient.

Also shown in Figure 4.1 (a-c), the 200 hPa austral summer jet maximum shifts south as it circulates east from the Dateline towards 120˚W. This results in a corresponding southerly progression of maximum vertical wind shear, and subsequently the most baroclinic environment. During winter (Figure 4.1d-f), the zonal wind maximum at 120˚W is located 10˚ further north than during summer, resulting in a jet stream contained within a narrow latitudional range (25˚S-35˚S). This seasonal change in orientation may help explain why the SPCZ is more diagonal during summer. Eastin and Vincent (1998) proposed instead that strong tropical convection produces upper-level divergent outflow which migrates south and enhances the jet stream through eastward curvature caused by the Coriolis force. Outflow from convection would also explain the parallel orientation of the subtropical jet to the SPCZ.

DJF cross sections (Figure 4.1a-c) show upper tropospheric westerly winds over the equatorial regions, especially at 150˚W and 120˚W. This corresponds to part of the Central Pacific "Westerly Wind Duct" mentioned by Webster and Holton (1982), which acts as a corridor for propagation of extratropical distrubances into the tropics. This duct may be a result of strong divergent outflow from West Pacific deep convection. During JJA (Figure 4.1d-f), the westerly winds retreat from the equator, probably because the maximum convection is now located around 10˚N. In essence, the westerly winds account for the upper branch of the Walker circulation discussed in Chapter 3. The relationship between SPCZ storminess and the Westerly Wind Duct on MJO timescales will be explored in Chapter 6.

4.2 Cross-Equatorial Flow

We now examine the presence of cross-equatorial flow and how it may increase instability in the tropical region. Observational (Tomas and Webster 1997) and modeling (Tomas et al. 1999) studies illustrate that convection is found away from the equator in regions with a strong cross-equatorial pressure gradient. A dramatic example of this is in the Indian Ocean Basin, during JJA, when the Asian Monsoon Circulation reaches its peak and the ITCZ is shifted far to the north. SLP gradients are comparatively weaker over the West Pacific (Figure 3.2), although we still find the lowest pressure over the warmest SSTs when convection in the SPCZ is greatest (12˚S during DJF [Figure 3.2a]). This weak gradient forces a mean northerly divergent wind maximum of about 3.5 ms^{-1} centered just north of the equator (Figure 4.2a). The cross-equatorial flow in this region causes a displacement of the zero absolute vorticity contour $(\eta = \zeta + f = 0)$ towards the summer (southern) hemisphere and creates an inertially unstable environment (Tomas and Webster 1997).

In the West Pacific, the SLP gradient (Figure 3.2b), divergent wind patterns (Figure 4.2b), and location of the $\eta = 0$ contour (thick black line) are reversed during JJA, when the SPCZ is closer to the equator and the ITCZ is located around 10˚N. The East Pacific ITCZ also responds dramatically to shifts in the location of the $\eta = 0$ contour. As evident in Figure 3.4c, the 925 hPa convergence pattern becomes amplified (strong convection) just west of the Isthmus of Panama during JJA, while the DJF (Figure 3.4a) East Pacific ITCZ is much weaker. Monthly-mean positions of the 925 hPa $\eta = 0$ contour are consistently found in the summer hemisphere, or along the equator in regions of weak meridional divergent winds.

a)

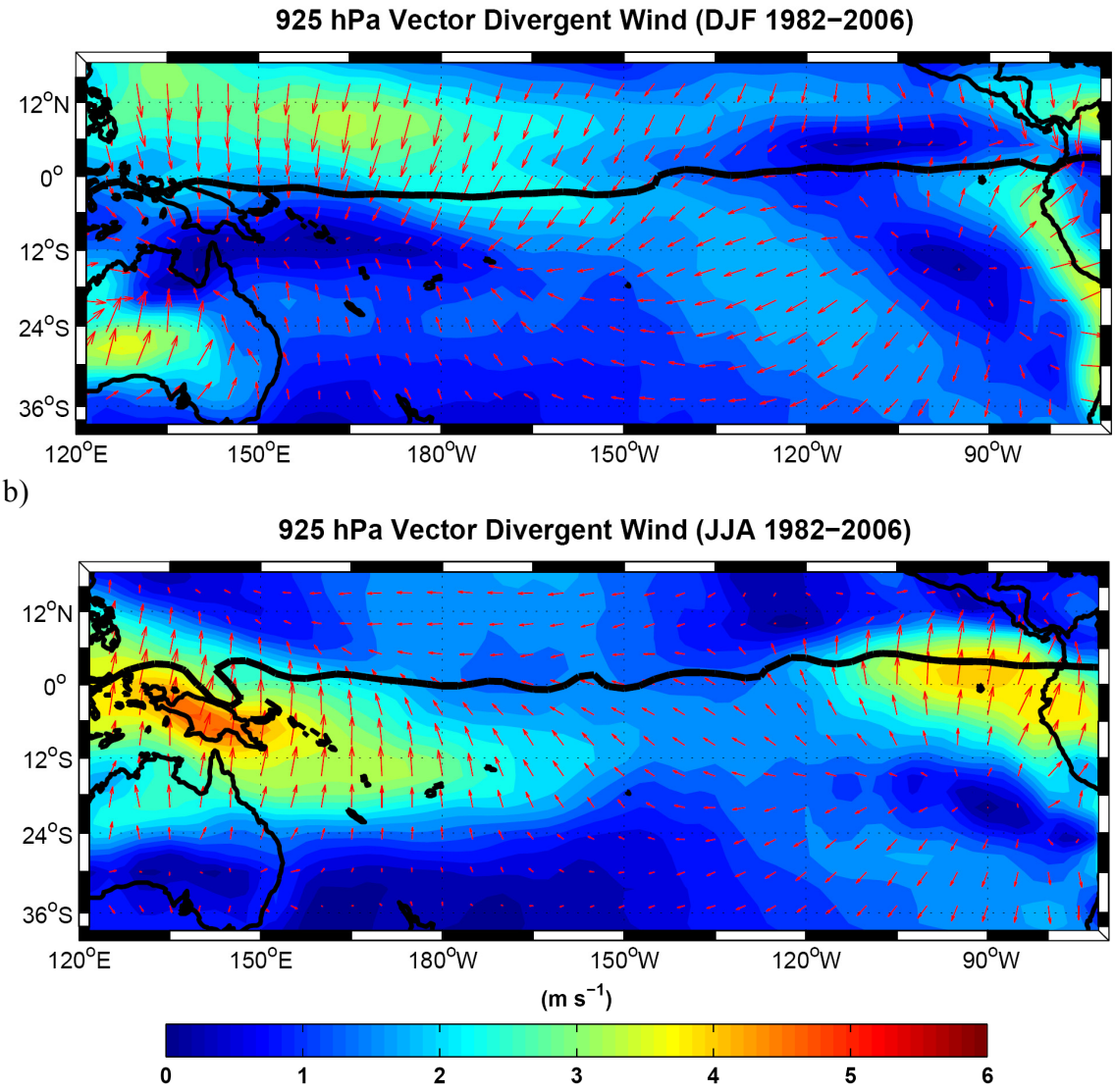

Figure 4.2 Seasonal averages of vector divergent wind (925hPa) during austral summer (a) and winter (b). Shaded contours indicate magnitude. Direction indicated by the red arrows. Zero absolute vorticity contour is indicated by the solid black line.

Tomas and Webster (1997) describe that an inertial instability is produced when a cyclonic circulation spins up to counteract the advection of anti-cyclonic vorticity by the cross-equatorial flow into the hemisphere of interest. We have created vertical cross-sections of the meridional divergent wind and divergence fields for the SPCZ (150˚E-

180˚E, Figure 4.3) during DJF (a,b) and JJA (c,d), to examine whether this idea can be applied to the West Pacific.

During DJF in the West Pacific, there is a strong northerly flow $\left(v_d \approx -5\ ms^{-1}\right)$ near the surface which extends from 25˚N to about 10˚S. A slightly weaker southerly flow $\left(v_d \approx +2\ ms^{-1}\right)$ originates in the SH mid-latitudes and meets the northerly flow. This accounts in part for the major boundary layer convergence $\left(\delta \approx -2x10^{-6}\, s^{-1}\right)$ observed in the tropics (Figure 4.3b). From 20˚S to 10˚N during DJF (10˚S to 20˚N, JJA), the mean winds are convergent up to the 400 hPa level, suggesting that deep convection is occurring (Karoly and Vincent 1999). In the upper troposphere, meridional winds are reversed and lead to a portion of the equatorial divergence which is stacked vertically above the surface layer convergence. Tomas and Webster (1997) theorize that this arrangement of meridional divergent winds forces positive absolute vorticity from the NH to the SH near the surface (below 850 hPa) and the reverse flow of negative absolute vorticity above 350 hPa. The zero absolute vorticity contour (Figure 4.3a, solid black line) agrees with this theory. In general, the divergent wind circulation and convergence/divergence dipole arrangements are reversed during the JJA months (Figure 4.3c and d) in the West Pacific. One interesting difference is that major boundary layer convergence in the ITCZ does not extend as far north from the equator in boreal summer as it does south during austral summer in the SPCZ. Vertical cross sections show a near surface meridional divergent wind flow, and subsequent transport of the $\eta = 0$ line away from the equator, that are less pronounced than over the Indian Ocean (not shown). Unlike the West Pacific analysis, occurring almost entirely over water, the Indian

subcontinent extends as far south as 15˚N and alters the meridional divergent wind flow due to surface heating differences (Webster et al. 1998).

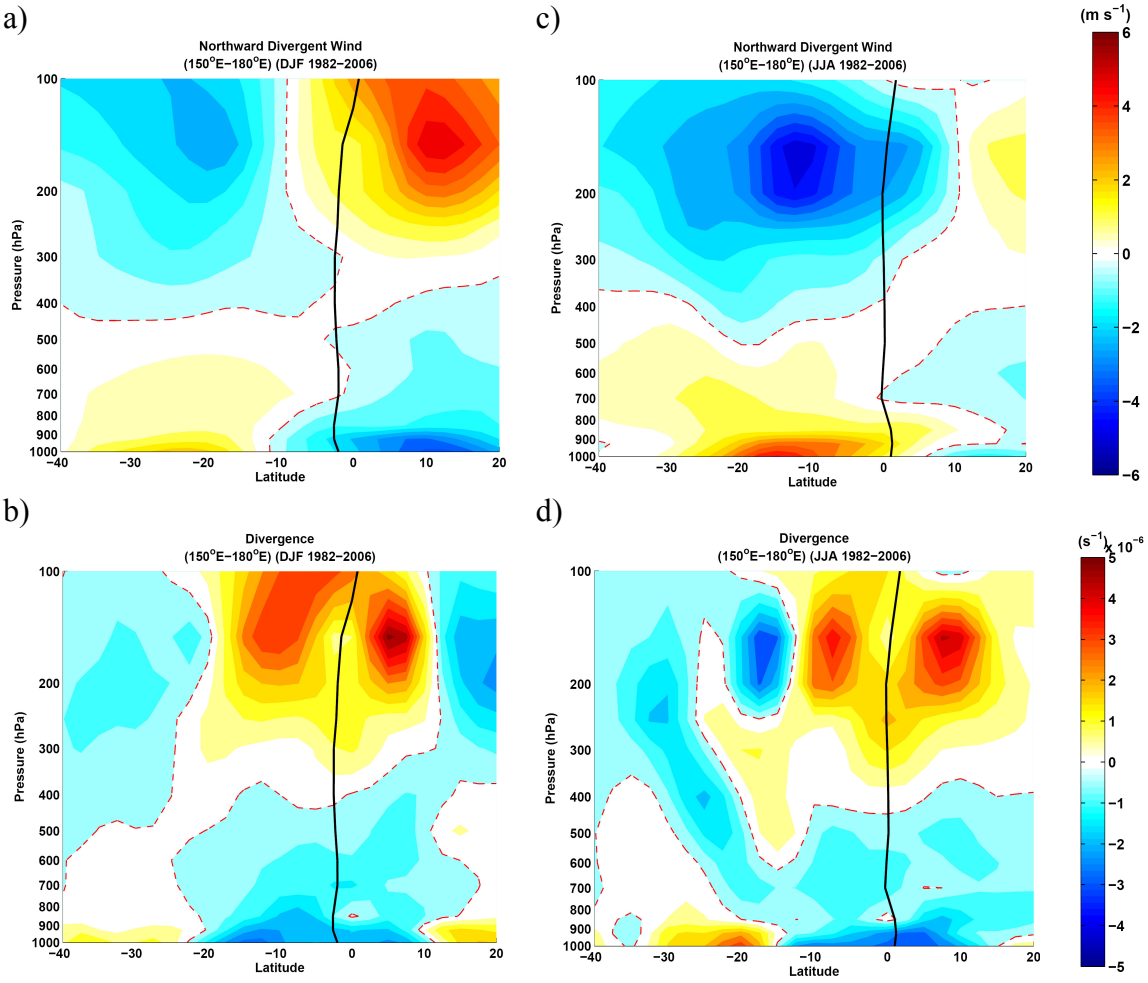

Figure 4.3 Northward divergent wind during DJF (a) and JJA (c). Divergence during DJF (b) and JJA (d). Zero contours indicated by the dashed red line. Zero absolute vorticity indicated by the solid black line in all plots. Region of interest is the West Pacific Basin (150˚E-180˚E).

Numerous studies have investigated the impact of meridional wind surges on tropical convection in the highly inertially unstable atmosphere of the Indian Basin (e.g., Fukutomi and Yasunari 2005). We now adapt Fukutomi and Yasunari's analysis to

determine the effects of individual cross-equatorial surges in the moderately inertially unstable West Pacific. A time series of daily DJF meridional winds at 850 hPa (v_{850}) averaged over a grid in the tropical Northwest Pacific (2.5˚N-17.5˚N, 155˚E-165˚E) is displayed in Figure 4.4a from 1982-2006 (dashed red line). Negative v_{850} is considered a measure of low-level surge activity and is likely caused by the passage of Rossby waves in the NH mid-latitudes (Fukutomi and Yasunari 2005). A 6-25 day bandpass filter (solid black line) is applied to the time series to remove influences from high frequency storms or the MJO. Superimposed on this plot is a ±1.5 standard deviation range of the filtered v_{850} time series. Minima falling outside of this range are considered strong southward surges (130 events during the 25 DJF seasons). Figure 4.4b shows only the 2006 season and provides a clearer look at the periodicity of southward surge events (minima around December 30th, January 15th, and February 2nd).

Dates of southerly surge events are used to compile a composite analysis of daily OLR anomalies (Figure 4.4c). The composite suggests that low OLR (strong convection) over the tropical and subtropical SPCZ is correlated with the occurrence of negative v_{850}. Negative OLR anomalies also occur over Northern Australia and across the Central Pacific, just south of the Hawaiian Islands. At the same time, positive OLR anomalies are found near the ITCZ region where the surge index is calculated. These anomalous regions are statistically significant at the 95% level determined using Student's t test. This suggests that the occurrence of southward surges have major impacts on convective processes, probably by advecting positive absolute vorticity into the SH and creating a more inertially unstable atmosphere. There is a striking similarity between these composite anomalies and the EOF analysis performed in Chapter 3.1 (Figure 3.5b).

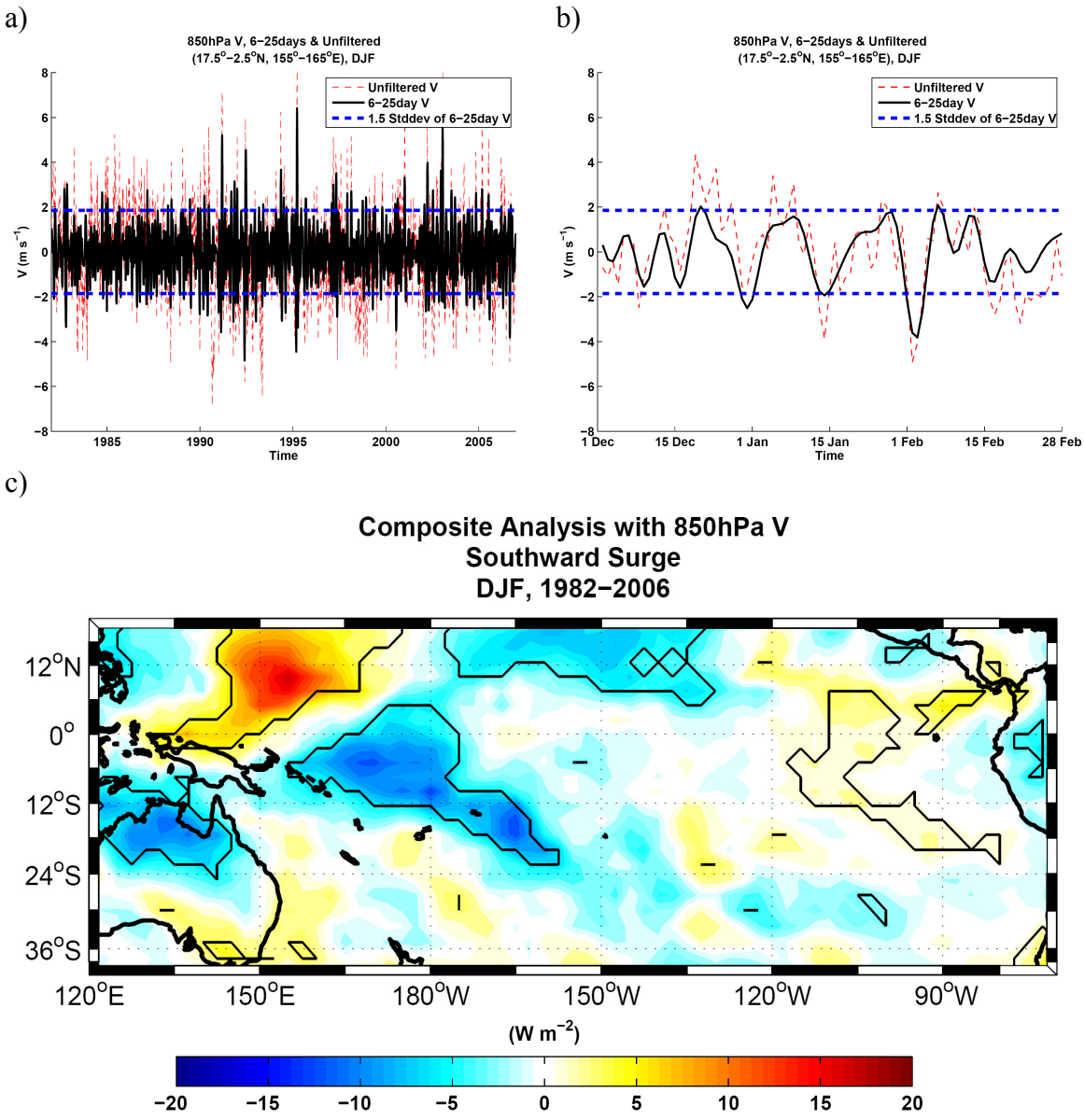

Figure 4.4 (a) Time series of 6-25 day filtered (solid black) and unfiltered (dashed red) 850 hPa meridional wind averaged over 2.5˚N-17.5˚N, 155˚E-165˚E during austral summer. Dashed blue lines indicate ±1.5 standard deviations from the filtered time series mean. (b) Same as (a) except only for 2006. (c) OLR composite anomaly during major southward surge events. Thin black lines enclose anomalies statistically significant at the 95% level.

Credence is given to the idea that dynamical processes, such as cross-equatorial wind surges, cause an oscillation on sub-monthly timescales between convective anomalies in the SPCZ and ITCZ. It remains unclear, however, whether the smaller negative OLR anomalies over the North Pacific are related to cross-equatorial surges over the West Pacific. The magnitude of OLR anomalies in the SPCZ region (10-20 Wm^{-2}) and large spatial extent (>$3x10^6$ km^2) suggests that the surge events may be responsible for significant variability of the regional Hadley and Walker circulations.

4.3 Wave Energy Accumulation

We have described the driving forces of the SPCZ as a combination of warm Southwest Pacific SSTs, the strong temperature gradient between the mid-latitudes and subtropics, and northerly divergent winds near the surface, shifting the zero absolute vorticity line south of the equator and creating an inertially unstable atmosphere. Now we investigate why the austral summer convection in the SPCZ is intense and has a large spatial footprint despite the similar SSTs (compared to the Northwest Pacific) and more inertially stable atmosphere than other major regions of off-equatorial convection. One possibility is that the SPCZ is enhanced by wave energy accumulation. The combination of SST distributions and location of the tropical continents (Africa, Australia, and South America) define the form of the Walker Circulation and introduce considerable negative zonal stretching deformation, $\frac{\partial u}{\partial x} < 0$, near regions of persistent storminess (Webster and Chang 1988).

Figure 4.5 reveals the seasonal mean SH zonal stretching deformation during DJF (a) and JJA (d) at the 925 hPa level. Negative (positive) values indicate that the zonal

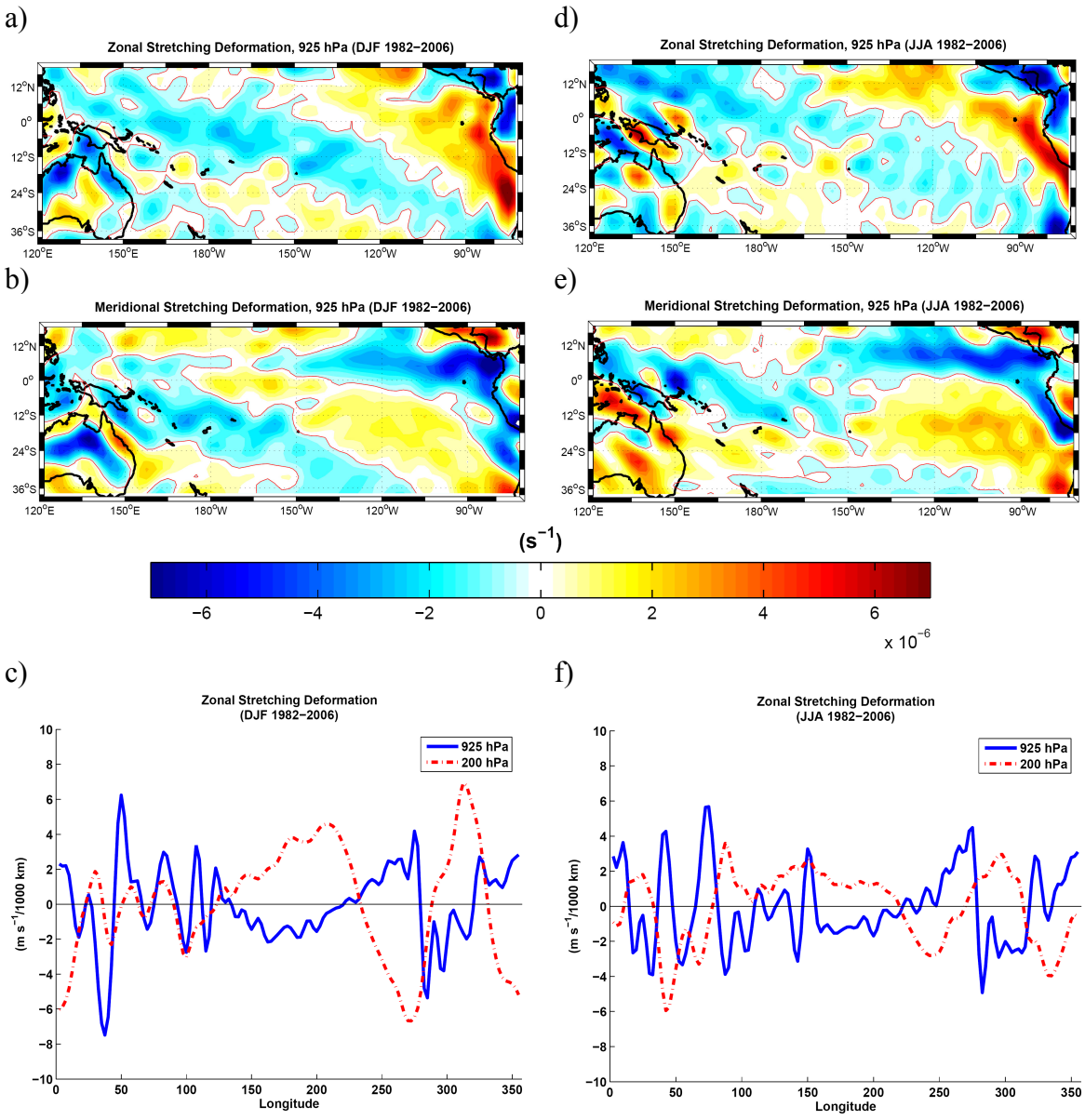

Figure 4.5 Seasonal averages of stretching deformation (925 hPa) during austral summer (zonal: a, meridional: b) and winter (zonal: d, meridional: e). The thin red line represents the zero contour. Zonal stretching deformation (m s^{-1}/1000 km) of the zonal wind at 925hPa (blue, solid) and 200hPa (red, dash-dot) during summer (c) and winter (f) averaged over equatorial latitudes (2.5˚N-2.5˚S).

flow is converging (diverging). The austral summer plot (Figure 4.5a) shows a diagonal region of $\frac{\partial u}{\partial x} < 0$ along and just to the east of the SPCZ, extending all the way from Indonesia to the southern tip of South America. Austral winter observations (Figure 4.5d) indicate that this diagonal pattern becomes weaker and shows a partial discontinuity over the central South Pacific. A likely mechanism for the weakening during JJA is the seasonal oscillation of warmer SSTs, and therefore also the Walker Circulation, towards the summer (northern) hemisphere. Observations of the NH have indicated that diagonal bands of $\frac{\partial u}{\partial x} < 0$ develop over the Northern Indian and Pacific Oceans, as well as Caribbean Sea during JJA, although NH convergence zones never become as pronounced as their SH (DJF) counterparts (Cocks 2003).

We now consider a simplified tropical atmosphere containing equatorially trapped Rossby and mixed Rossby gravity waves emanating from energy sources such as large latent heat releases associated with cumulonimbus cloud systems or other regions of instability. Webster and Chang (1988) discuss the impact of a zonally varying basic state on the phase and group velocity (C_{gd}) of a Rossby wave and demonstrate that the longitudinal C_{gd} may only go to zero in regions of negative zonal stretching deformation. In regions where $\frac{\partial u}{\partial x}$ is negative, the wave number of the incident wave increases and C_{gd} approaches zero, forcing the wave to become longitudinally trapped (Webster and Chang 1997, their Figure 15). This has important consequences about the region where wave energy (ε), defined by Equation 8 (where h is the wave height, g is gravity, and ρ is the atmospheric density), will tend to accumulate.

$$\varepsilon = \frac{\rho g h^2}{2} \tag{8}$$

Webster and Chang (1997) analytically reveal that ε can grow exponentially with time in negative stretching regions by developing the following equation:

$$\frac{\partial \varepsilon}{\partial t} + C_{gd} \frac{\partial \varepsilon}{\partial x} = -\varepsilon \frac{d\overline{u}}{dx} \tag{9}$$

Meridional stretching deformation also appears to support formation of the SPCZ (Kodama 1993). Plots of $\frac{\partial v}{\partial y}$ during DJF and JJA are shown in Figures 4.5b and e, respectively. During austral summer, a band of negative meridional stretching deformation exists to the southwest of the main SPCZ OLR minima. The pattern has a similar area extent and magnitude as the $\frac{\partial u}{\partial x} < 0$ band. It appears that the poleward boundary layer flow over the Southwest Pacific leads to significant convergence along the western SPCZ. In winter, $\frac{\partial v}{\partial y} < 0$ is oriented more parallel to the equator and associated with the ITCZ. This is especially true over the East Pacific where the strong low-level equatorial flow converges and supports a vigorous Hadley cell. Questions remain about how regions of $\frac{\partial v}{\partial y} < 0$ influence the meridional propagation of wave energy.

This study confirms that there is negative zonal stretching deformation throughout the western half of the equatorial Pacific (120˚E to 220˚E) at the 925 hPa level during DJF (Figure 4.5c). Further east, $\frac{\partial u}{\partial x}$ becomes positive suggesting wave energy emanation near the surface, thus less convection than in the West Pacific. Webster and

Holton (1982) note that maximum poleward energy propagation from the tropics occurs in these regions of minimal convection and upper tropospheric westerly winds. The corresponding 200 hPa plot during DJF (Figure 4.5c) shows that $\frac{\partial u}{\partial x}$ is negative in the East Pacific (230˚E to 280˚E), allowing energy to accumulate in the upper troposphere before propagating away from the equator. Figure 4.6 shows a schematic of waves forced by convective regions (such as the SPCZ) and emanating out of the tropics in the Westerly Wind Duct. The magnitude of zonal stretching deformation at the 925 hPa and 200 hPa levels is smaller during JJA (Figure 4.5f). This is expected due to the weakening of the Pacific Walker cell during DJF. Tomas and Webster (1994) show that upper tropospheric westerlies in this region allow disturbances to move from the extratropics to the tropics, and occasionally across the equator. Examination of impacts from SPCZ convection on the Walker Circulation and the influence this has on teleconnections will be discussed further in Chapter 6.

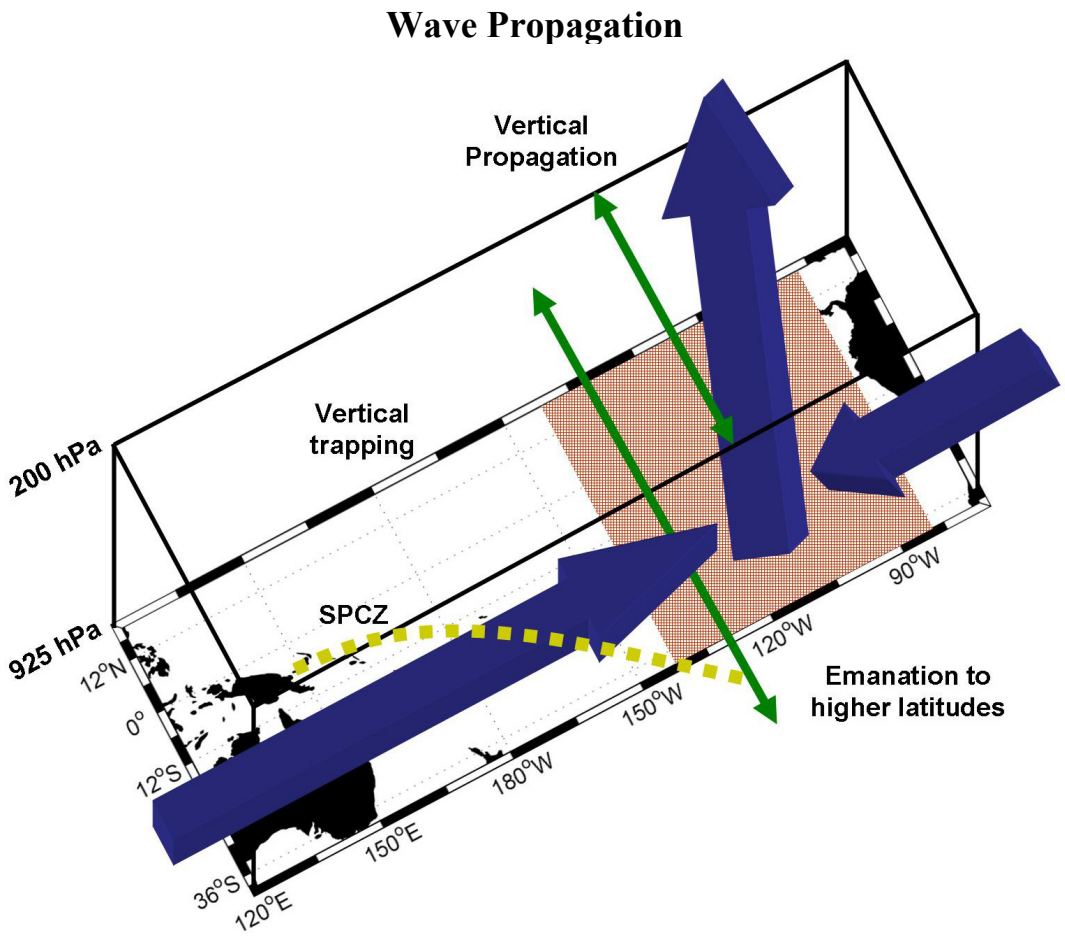

Figure 4.6 Schematic diagram of wave propagation in and out of the Westerly Wind Duct (red box). The diagram shows the three-dimensional trajectories of waves (blue arrows) forced in the convective regions of the Pacific Basin, such as the SPCZ (yellow dashed line). Meridional and vertical emanation zones indicated by green arrows. Schematic adapted from Webster and Chang (1997).

CHAPTER 5

MODES OF VARIABILITY

Thus far, we have described the important dynamics of the SPCZ. Seasonal comparisons indicate that convective activity dictates maximum storminess occurring in the SPCZ during DJF. The next task in our classification of the SPCZ is to explore other major modes of variability on shorter (e.g., sub-monthly and MJO) and longer (e.g., ENSO) timescales and how they help define the region. We again accomplish this by using low OLR observations as an indication of deep tropical convection. However, the focus will now turn to identifying significant timescales of variability. Wavelet analysis techniques (Torrence and Compo 1998; Cromwell 2001; Grinsted et al. 2004) allow us to determine when, and in which portions of the SPCZ, major modes of variability occur. Fourier decomposition methods are used to extract MJO frequencies from the OLR data set and determine when they influence storm development in the tropics. Results of these filters will provide specific time periods to use in compiling subsequent composites of the MJO in Chapter 5.2.

We begin our investigation of West Pacific OLR variability by noting that the largest departures from the austral summer mean occur in regions of maximum storminess, including the tropical and subtropical SPCZ, northern coast of Australia, NH Warm Pool, and ITCZ. Figure 5.1a shows the standard deviation (SD) from 25 DJF seasons of OLR data (1982-2006), clearly indicating that the highest variance occur over these regions. One exception to the correlation between high storminess and variance is over the Indonesian Archipelago where land-sea interactions may increase the local

vertical updraft velocities and result in abundant cloudiness and more consistent low daily OLR values (Cocks 2003).

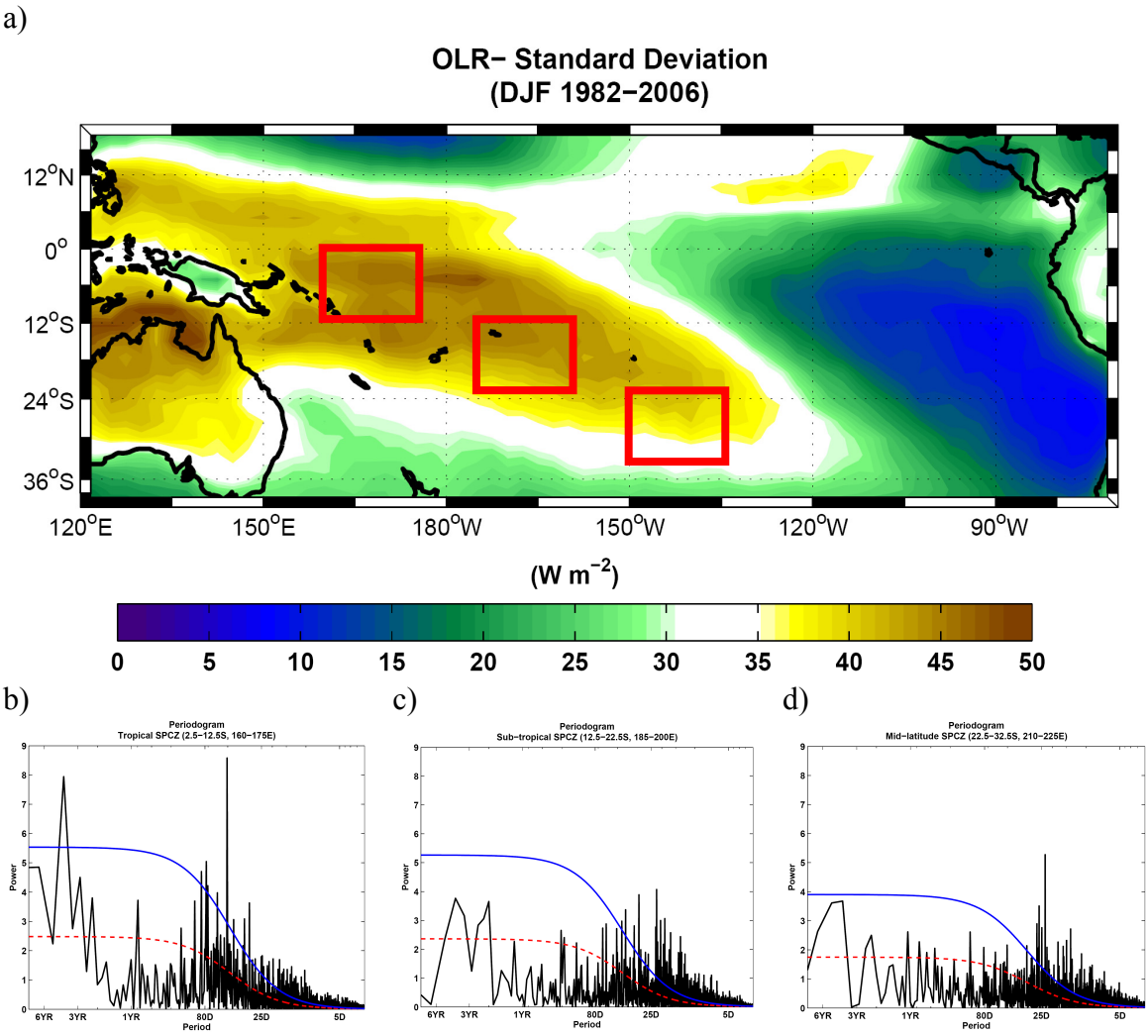

Figure 5.1 (a) Standard deviation (W/m^2) of unfiltered daily OLR time series from 1982-2006 during DJF. Warmer (cooler) colors represent regions of higher (lower) variability. Fourier power spectra of OLR in the tropical (b), subtropical (c), and mid-latitude (d) regions of the SPCZ (red boxes). The lower dashed line is the mean red-noise spectrum for a lag-1 autocorrelation of .77 (b), .76 (c), and .69 (d). The upper solid line is the 95% confidence spectrum. OLR data has been filtered to remove any annual cycles and de-trended. An eleven point running mean was applied to the OLR spectrum.

Power spectra of daily OLR time series (filtered to remove any annual cycles and long-term trends) for the tropical, subtropical, and mid-latitude SPCZ regions are shown in Figures 5.1b, c, and d, respectively. Areas under the solid black lines indicate the amount of power explained by each particular period range (Hartmann 2005). The results are normalized and displayed on a log (period) scale to improve visual interpretation. Red noise power spectra (dashed-red lines) for a lag-1 autocorrelation of .77 (b), .76 (c), and .69 (d) along with the corresponding 95% confidence level (solid blue) are overlaid on the plots using the methods of Torrence and Compo (1998). The tropical spectrum shows significant periods in the synoptic (2-8 day), intraseasonal (25-80 day) and interannual (3-5 year) timescales. There is also a broad range of significant periods between the synoptic and intraseasonal bands (10-25 days), suggesting that there are often convective oscillations, one to two weeks in duration. Schnadt et al. (1997) found a similar spectral peak during a study of Northwest Pacific OLR, which they attribute to westward propagating convective disturbances and occasional recurrence of tropical cyclones (TCs). In the subtropical and mid-latitude portions of the SPCZ, the interannual variability is not significant at the 95% level; however, it is still above the red noise spectrum. We also see that the intraseasonal variability is weaker than in the tropics and shifted towards the higher frequency range (25 days), especially in the mid-latitudes. OLR variability from synoptic type disturbances is significant in the subtropics and mid-latitudes as well. For the remainder of this section, we will discuss these individual groupings in greater detail.

5.1 Sub-monthly Scales

The power spectra in Figure 5.1b-d lack the ability alone to indicate when each particular OLR periodicity tends to occur. For instance, we know that convection varies on synoptic and MJO timescales in the tropical SPCZ, at least when averaged over 25 years, but we do not know if these frequencies occur more often than the mean during particular years. To answer this question, we employ wavelet transform techniques to determine where, and when, each period of variability is significant. Using the methods of Torrence and Compo (1998), continuous wavelet transforms for one year of OLR (2005) are shown in Figure 5.2 for the tropical (a), subtropical (b), and mid-latitude (c) regions. Only one year is used in this case to focus attention on sub-monthly variability and a particular MJO event (March-May, MAM 2005), although it will be shown later that this represents a typical year. Synoptic variability significant at the 95% level, indicated by solid black contours, is observed in each region and season. We also note that the MJO periodicity, first observed in the tropical region just inside the cone of influence (COI) line (MAM), seems to progress into the subtropics by late in the austral fall with a slightly longer period of about 55 days. We will briefly examine how convection propagates between different regions of the SPCZ before our attention shifts entirely to specific MJO impacts in the West Pacific.

Power Hovmoller plots of 6-25 day variability (as described by Torrence and Compo 1998; Cromwell 2001) are displayed in Figure 5.3, subplots I-III for 120˚E-240˚E in the tropical, subtropical, and mid-latitude SH (2005). Zonal averages of sub-monthly variability peaks in the tropics during the transitional fall and spring months, which is an expected result of mid-latitude cyclonic disturbances propagating into the low latitudes

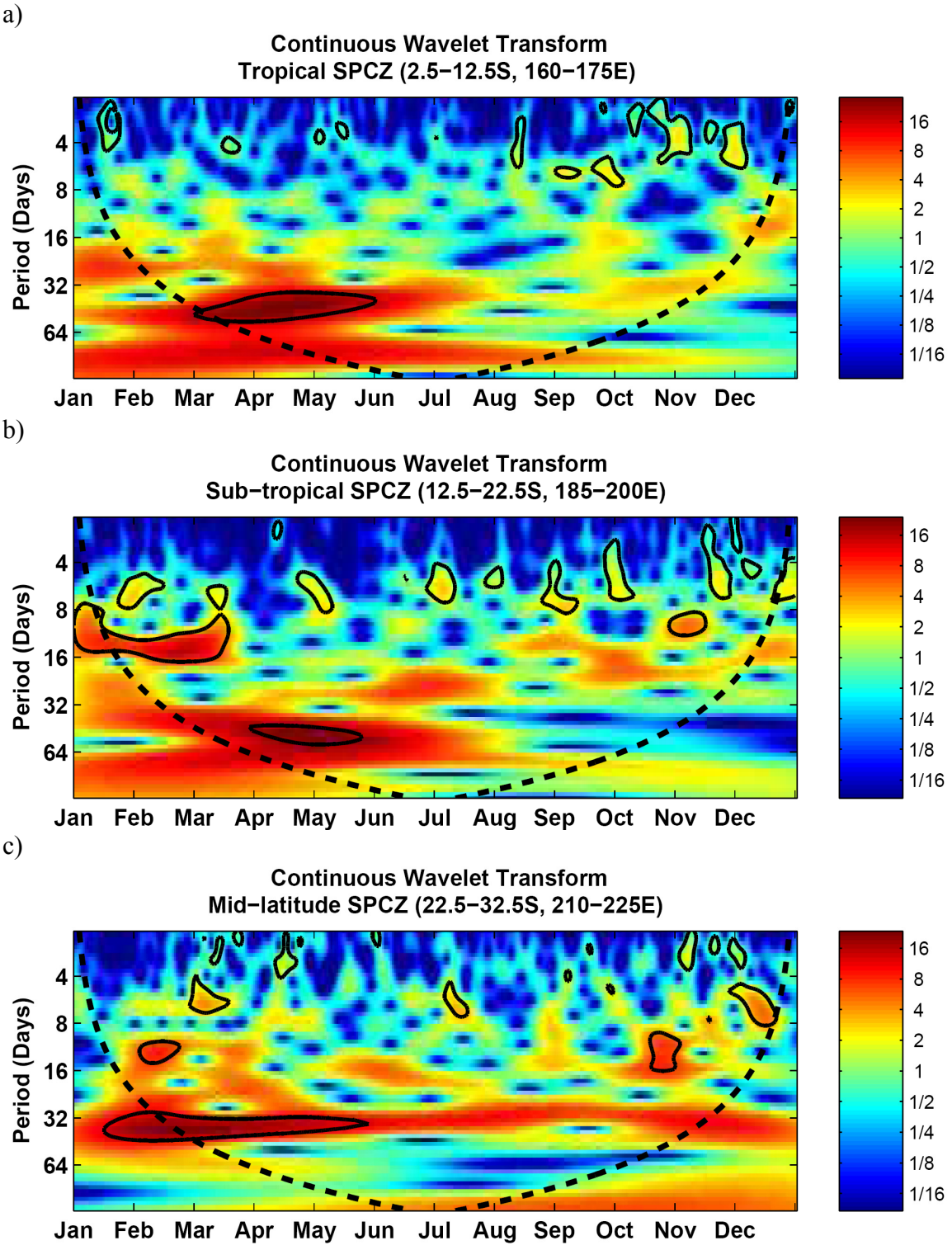

Figure 5.2 Continuous wavelet transforms of OLR during 2005 in regions representative of the tropical, 2.5˚S-12.5˚S (a); subtropical, 12.5˚S-22.5˚S (b); and mid-latitude, 22.5˚S-32.5˚S (c) portions of the SPCZ. Solid black lines enclose regions statistically significant at the 95% level. Regions below the dashed black lines are subject to edge effects.

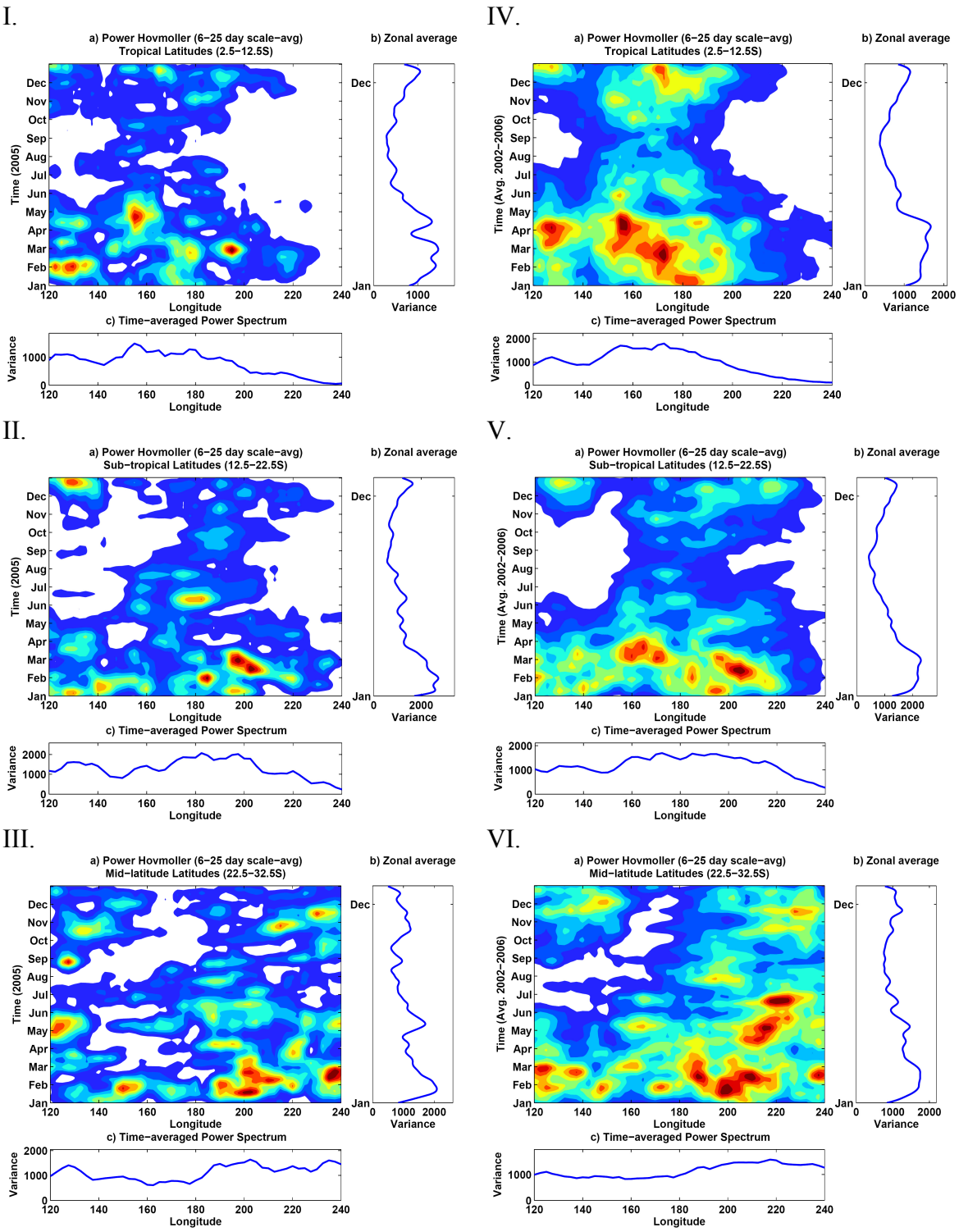

Figure 5.3 Sub-plots I through VI: (a) Power Hovmoller diagrams of 6-25 day averaged wavelet powering OLR; (b) the average of (a) over all longitudes; (c) the average of (a) over all times. The original OLR one year time series during 2005 (I, II, III) are from 2.5˚S-12.5˚S, 12.5˚S-22.5˚S, and 22.5˚S-32.5˚S; respectively. Plots IV, V, and VI are equivalent five year means of Power Hovmoller diagrams from 2002 to 2006.

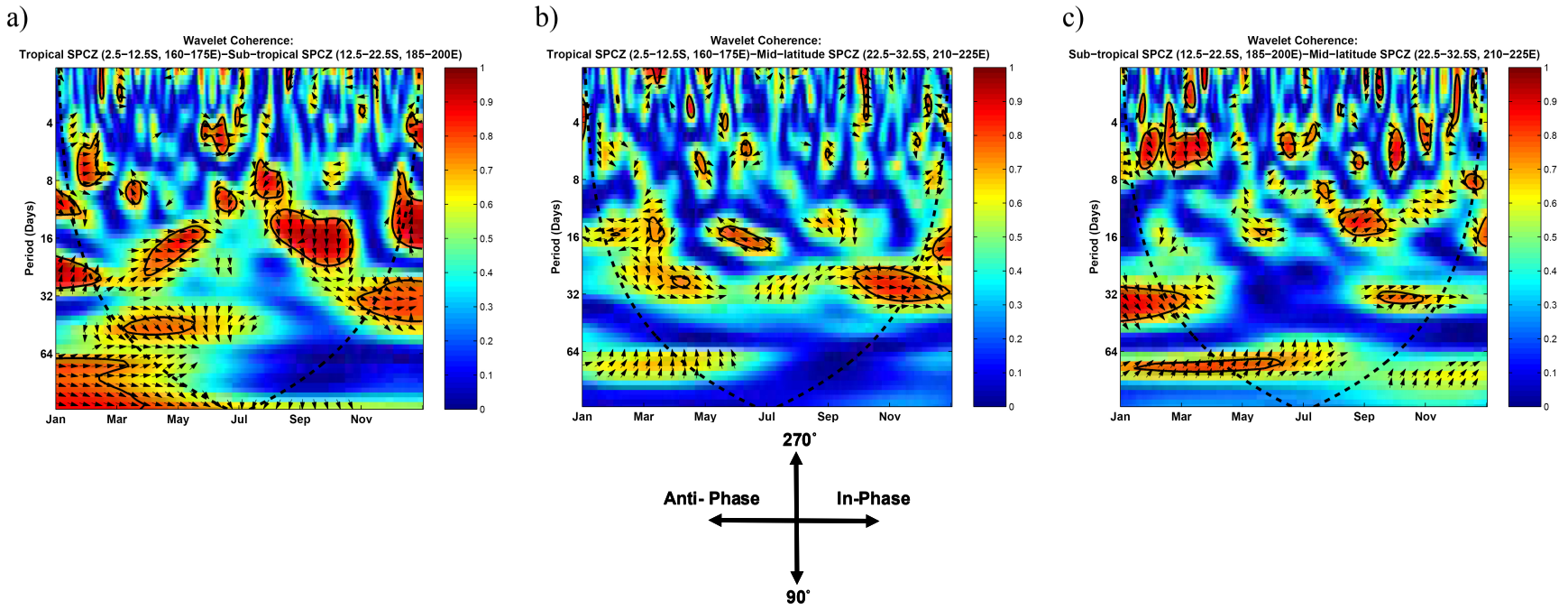

Figure 5.4 Squared wavelet coherence between OLR time series during 2005 between the tropical and subtropical (a), tropical and mid-latitude (b), and subtropical and mid-latitude (c) regions of the SPCZ. The thick, black contours enclose regions of greater than 95% confidence against a red-noise process. Regions outside the dashed, black lines are in the "cone of influence" where edge effects may distort the data. Arrows indicate the relative phase relationships (with in phase pointing right, anti-phase pointing left, and the first time series leading the second pointing straight down).

(Cocks 2003). Support for this comes from wavelet coherence analysis (as in Grinsted et al. 2004) of tropical and mid-latitude OLR which shows significant anti-phase relationships of 6-25 day variability (Figure 5.4b). Subtropical 6-25 day variability peaks during the austral summer months (Figure 5.3, subplot II), and shows coherence with the mid-latitudes (Figure 5.4c) during these times. The zonal average mid-latitude variability has less of a seasonal cycle, although the five year average suggests that peak intensities become more concentrated in the 200-220˚E longitude band during austral fall. Averages of five years (2002-2006) show similar results to the patterns from 2005 (Figure 5.3, subplots IV-VI).

5.2 Madden-Julian Oscillations

One final observation gained from the wavelet coherence analyses concerns OLR periodicities longer than 25 days. Convection at these timescales in the tropics seems to lead that in the subtropics (Figure 5.4a) by a phase of 45˚ during MAM of 2005, while the tropical relationship with the mid-latitudes (Figure 5.4b) shows no significant coherence. During austral fall (MAM), the MJO event that was diagnosed from Figure 5.2a seems to be associated with significant interactions between the tropics and subtropics. Observing that the typical periodicity of this wave is about 50 days, we calculate from the coherence phase relationship that it takes about six to seven days for the MJO signal to propagate from the tropical to subtropical SPCZ. While the continuous wavelet transform of mid-latitude OLR (Figure 5.2c) also shows significant variability with a similar period, there does not appear to be any coherence of MJO signals between the tropics or subtropics with the mid-latitudes (Figure 5.4b or c).

Coherence with the mid-latitudes does seem possible on longer timescales (periods > 65 days). The significance of this relationship exceeds the 95% threshold for signals propagating from the subtropics during February through early June of 2005 (Figure 5.4c). The nearly in phase nature of the coherence suggests that a similar mechanism is forcing nearly simultaneous convective anomalies in both regions. Caution must be applied to this particular result because large portions of the statistically significant areas occur outside the COI, and could be severely distorted by edge effects. There are also no significant periodicities greater than 65 days in the continuous wavelet transforms during 2005 (Figure 5.2), further discounting this coherence relationship. We leave additional study of low-frequency relationships with the mid-latitude SPCZ to a more comprehensive wavelet analysis.

While questions remain about how convection associated with the MJO moves through the SPCZ, Figures 5.1b-d illustrate that the 25 year average of 25-80 day variability is significant at the 95% level in the tropics and subtropics. Continuous wavelet transforms of 1982-2006 OLR also show that there is significant 25-80 day variability (within the solid blue lines) almost every year in these regions (Figure 5.5a and b), along with occasional bursts in the mid-latitudes (Figure 5.5c, e.g., austral summer of 1990). Power Hovmoller diagrams using scale averages of these periods show that the variability peaks in the tropical SPCZ longitudinal range (160˚E-175˚E), while it is much broader in the subtropics (Figure 5.6). The plot of the mid-latitudes show a minimum in the time-averaged power between 160˚E-180˚E which is a region just north of New Zealand that commonly experiences clear conditions, even during MJO events (Matthews et al. 1996). An interesting observation from the Power Hovmoller

a)

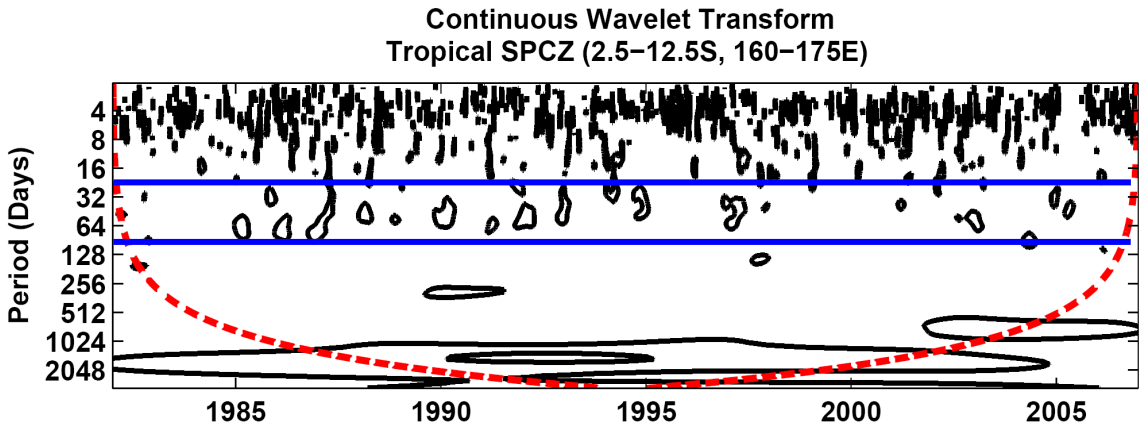

b)

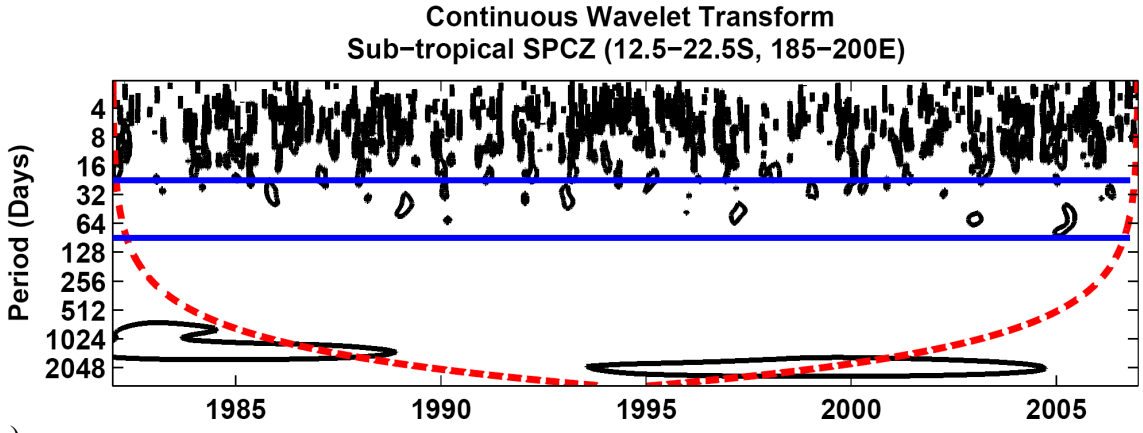

c)

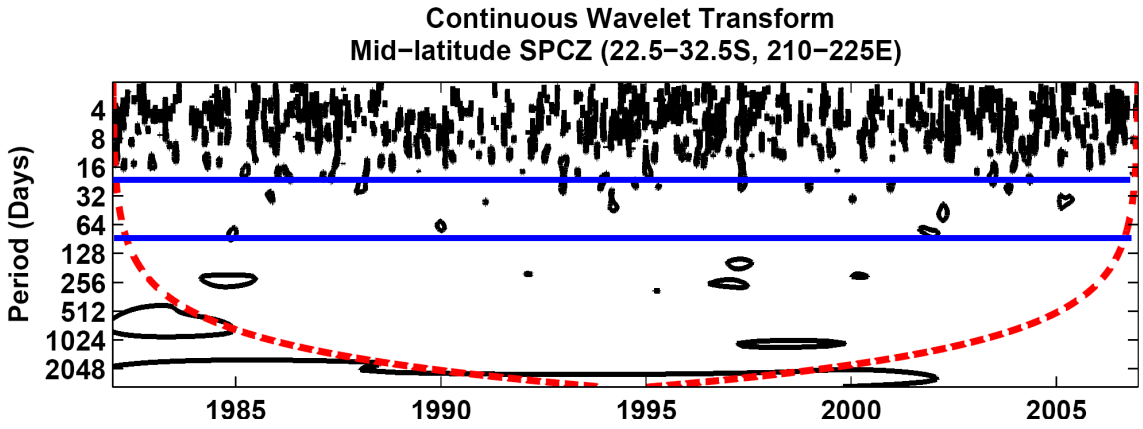

Figure 5.5 Continuous wavelet transforms of OLR during 1982 to 2006 in regions representative of the tropical, 2.5˚S-12.5˚S (a); subtropical, 12.5˚S-22.5˚S (b); and mid-latitude, 22.5˚S-32.5˚S (c) portions of the SPCZ. Solid black lines enclose regions statistically significant at the 95% level. Blue lines enclose variability on 25-80 day time scales. Regions below the dashed red lines are subject to edge effects.

I.

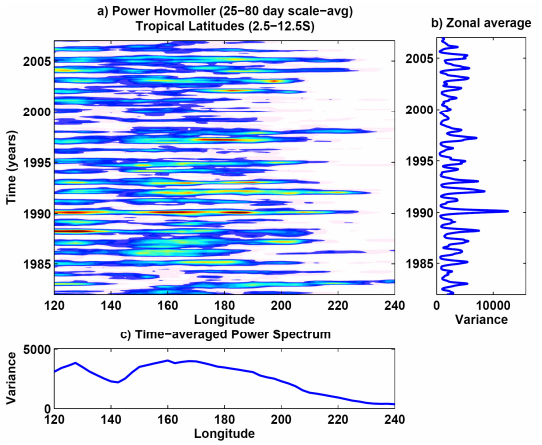

II.

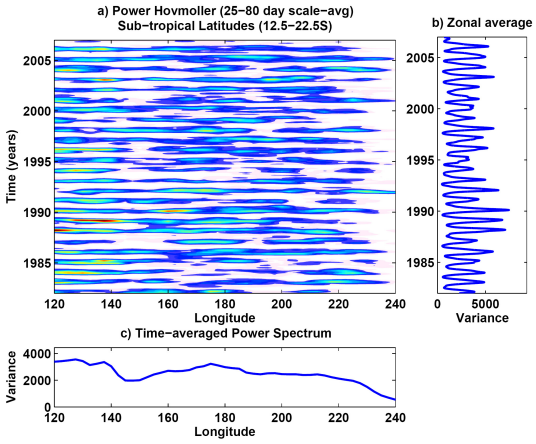

III.

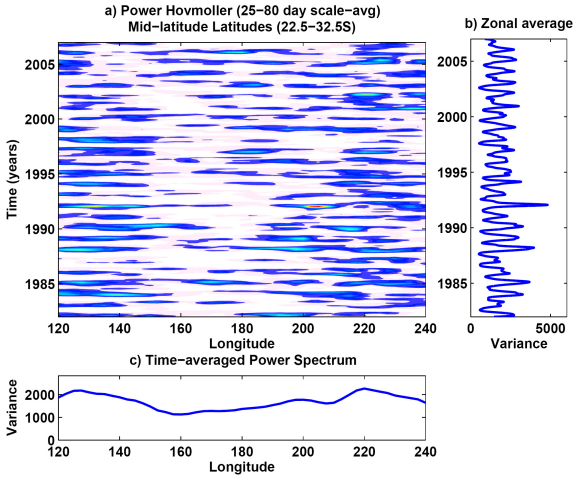

Figure 5.6 Sub-plots I through III: (a) Power Hovmoller diagrams of 25-80 day averaged wavelet powering OLR; (b) the average of (a) over all longitudes; (c) the average of (a) over all times. The original OLR time series during 1982-2006 (I, II, III) are from 2.5˚S-12.5˚S, 12.5˚S-22.5˚S, and 22.5˚S-32.5˚S; respectively.

(Figure 5.6I) is that MJO convection at tropical latitudes is more likely to propagate into the Central Pacific during major El Niño events, a known condition for enhanced eastward MJO propagation. Support for this observation comes from conducting a continuous wavelet transform of OLR over the Central Pacific (10˚S, 140˚W) and observing the 25-80 day scale-averaged time series for peaks corresponding with El Niño events (not shown). Three of the peaks were observed to correspond with the 1983, 1992, and 1998 El Niños.

We have shown that there are significant modes of variability in the SPCZ ranging from synoptic to interannual timescales. Within this range, 25-80 day MJOs are observed most years in the tropical and subtropical SPCZ, and occasionally into the mid-latitude SPCZ or tropical Central Pacific. We also noted that the spatial extent of this variability is linked to slow oscillations in the Pacific, such as ENSO.

The OLR power spectrum and wavelet analyses have left us with questions about where mesoscale convective systems (MCSs) originate and what dynamical processes determine how they interact with the SPCZ. To address these questions we briefly discuss a typical MJO cycle using an EOF analysis of 25-80 day filtered OLR data extending from 1982 to 2005, with the methods discussed by Matthews (2000). Definitions of MJO events using this band pass filter range are based on the results of the OLR power spectrum, from the tropical SPCZ, discussed earlier. Previous studies used filters to extract MJO variability, such as 30-96 days (Wheeler and Kiladis 1999), 20-200 days (Matthews 2000), or 20-100 days (Benedict 2005). Matthews (2000) justifies the need for a much wider bandwidth to avoid problems of successive MJO events merging

into one another; however, our interest is not to discern individual events, but instead composite a 24 year mean (1982-2005) of how the SPCZ responds to strong MJOs.

Spatial structures of the first two EOFs are presented in Figure 5.7. These leading two eigenvectors explain 8.2% and 6.5% of the variance, respectively and are well separated from higher EOFs, which mostly constitute sampling noise. EOF 1 (Figure 5.7a) shows negative OLR anomalies in the Central Indian Ocean and positive anomalies over the West Pacific Warm Pool and SPCZ region. Negative OLR anomalies in EOF 2 (Figure 5.7b) are centered over the West Pacific, while positive anomalies have become established over Africa and the Western Indian Ocean. These convective dipole patterns are similar to the results Matthews (2000) achieved using a broader bandwidth filter. Time series of the first and second PCs are calculated by projecting the EOF spatial structures onto the filtered OLR fields (Figure 5.7c and d). We show a six month (January 1, 2005 to June 30, 2005) subplot in Figure 5.7c to demonstrate that PC 1 leads PC 2 by about a quarter of a cycle. This time section is chosen to match the detection of MJO variability in the continuous wavelet transform of OLR data (Figure 5.2). The 90˚ lag of PC2 suggests that convection typically takes about 15 days to propagate from the Indian Ocean to Indonesian Archipelago during a 60 day MJO (e.g., Benedict 2005).

Dates of strong MJO events interacting with the SPCZ, extending from January 1, 1982 to December 31, 2005, can be identified using the PC 2 time series (Figure 5.7d), as it clearly reveals peaks in convection closest to the Southwest Pacifc. Positive amplitudes above one SD are considered strong events for purposes of this study. Using this threshold, we isolate 58 peaks over the 24 year time series. Because the tropical and subtropical regions of the SPCZ are most active during the austral summer months, we

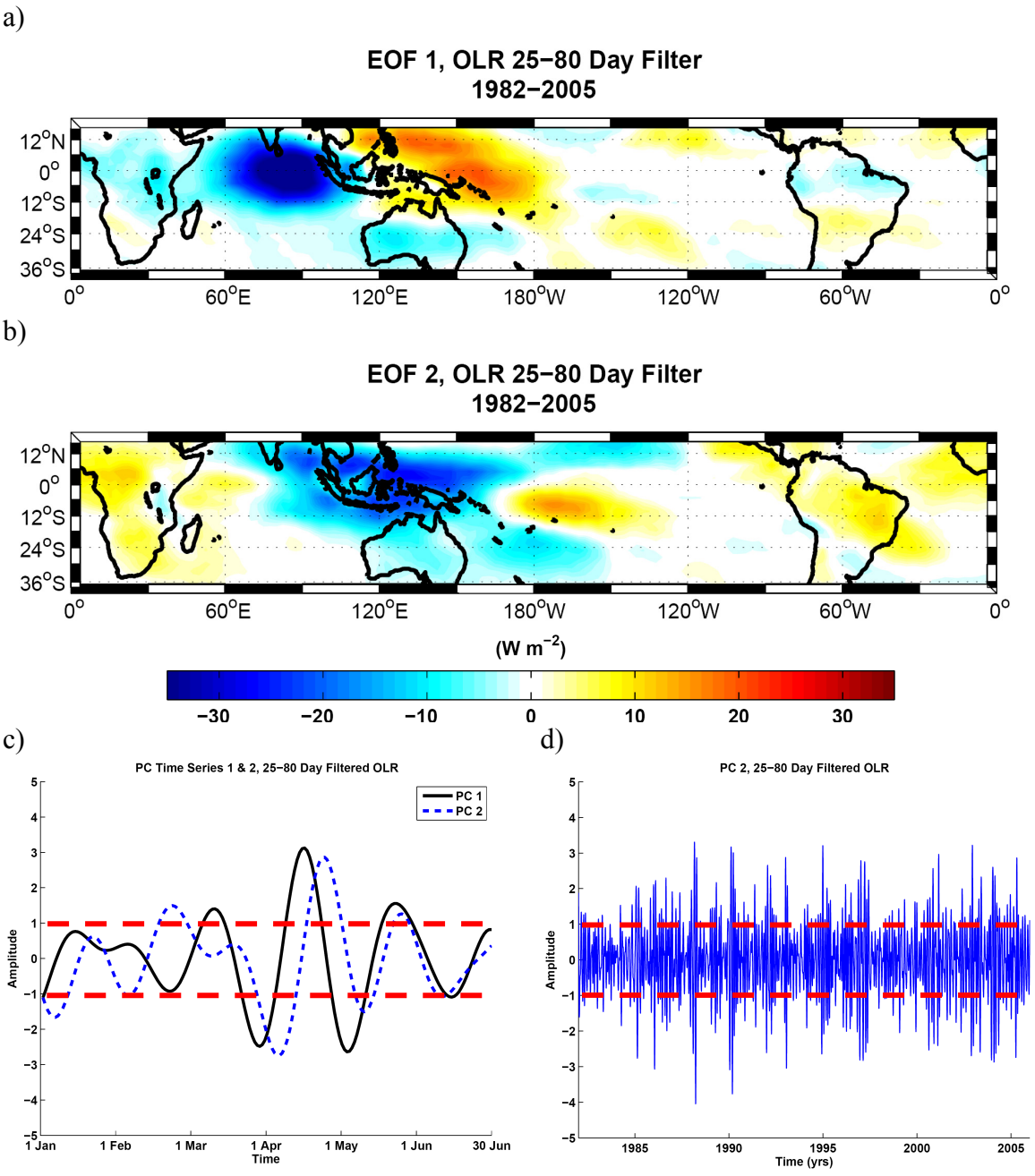

Figure 5.7 Empirical orthogonal function (EOF) analysis of 25-80 day filtered OLR: (a) EOF1, (b) EOF2. (c) PC1 (solid black) and PC2 (dashed blue) of the EOF analysis from January 1, 2005 to June 30, 2005. (d) PC2 of the entire EOF time series. Dashed red lines indicate ±1 standard deviation.

limit our events to those occurring in DJF, leaving 12 dates of strong MJO events for composite analysis.

Anomalous OLR composites from 25 days prior to 20 days after the date of maximum DJF peaks of the second PC are shown in Figure 5.8 in increments of 5 days. Positive anomalies are found throughout the equatorial Indian and West Pacific Oceans 25 days prior to the peak MJO activity over Indonesia. There appears to be no evidence of the MJO convective dipole pattern at this time. Within ten days, anomalous convection (negative OLR) has formed over most of the western Indian Ocean and continues to amplify and spread gradually east through the basin. By day 0, peak negative OLR values are now centered over Indonesia, while positive anomalies are found over the western Indian Ocean. At this time, the tropical and subtropical SPCZ is experiencing above normal OLR. Negative OLR anomalies appear further southeast in the mid-latitude SPCZ. This signal may be associated with advection of relative vorticity in front of the main MJO convective envelope (Meehl 2001). The day 0 plot is similar to the second EOF spatial pattern with anomalous convection over Indonesia and the mid-latitude SPCZ, as well as less cloudy than normal conditions over most of the Indian Ocean. At days +10 to +15, convection has shifted further east, with the strongest anomalies located in the SPCZ. Figure 5.8b indicates that much of the negative anomalies in the SPCZ are statistically significant at the 95% level, using a two tailed Student's t test for $N = 12$ independent samples. The remaining lag composite (day +20) illustrates that anomalous clear conditions continue to propagate eastward from the Central Indian Ocean, through Indonesia, and into the western SPCZ. Meanwhile, the convective region moves southeastward along the diagonal SPCZ, as observed by Zhang

and Dong (2004). During this period, the convective peak remains centered close to the Dateline, while weaker negative anomalies are observed throughout the equatorial and subtropical South Pacific.

a)

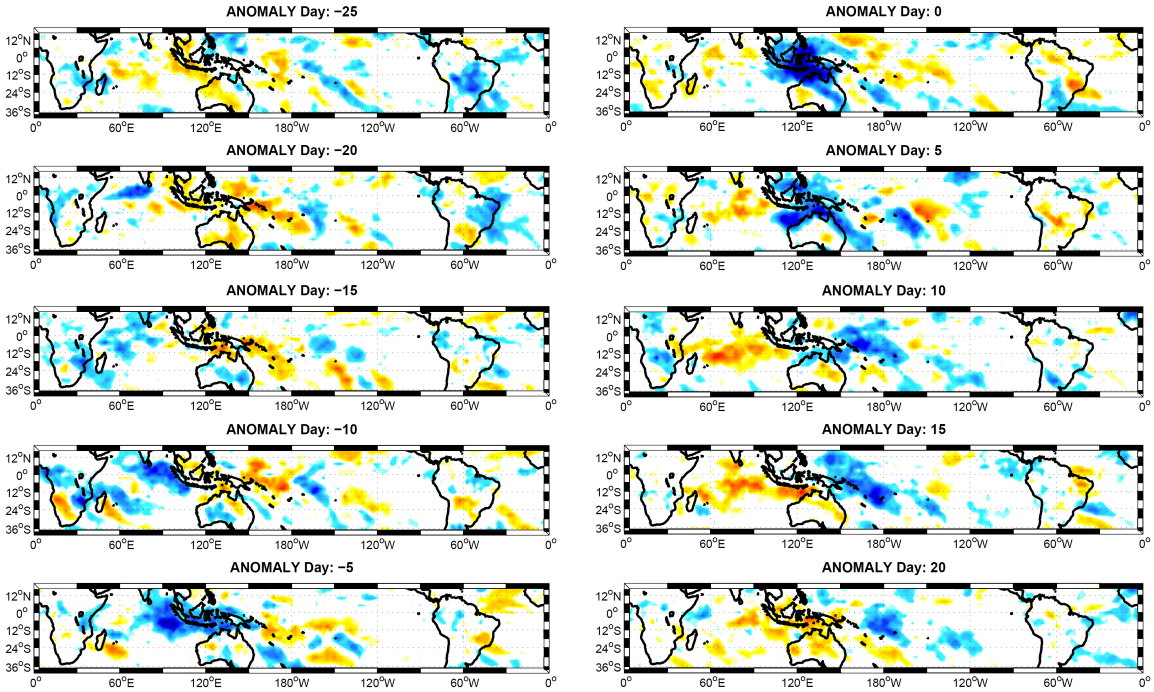

b)

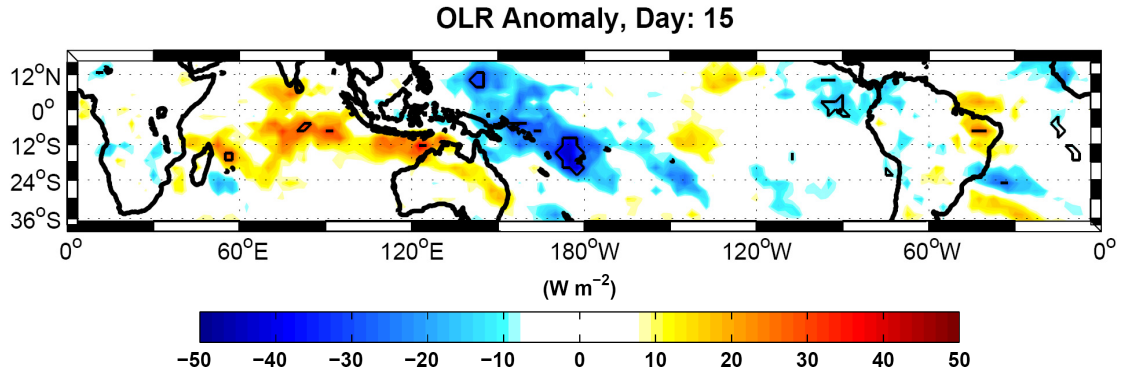

Figure 5.8 (a) Lead/lag composite OLR anomalies during major MJO events occurring in DJF from 1982 to 2005. (b) OLR composite anomaly 15 days after the maximum peaks of filtered DJF OLR values in the Indonesian region. Thin black lines enclose anomalies statistically significant at the 95% level.

A similar composite analysis of zonal winds at the 925 hPa level is also performed (not shown). In general, easterly anomalies (negative values) initially are found across the Equatorial Indian and West Pacific (day -25). These are gradually replaced by westerly winds that slightly lag behind the propagation of convection over the Indian Ocean and correlate with positive convective anomalies over the Pacific. This supports the results of Benedict (2005) who showed that the westerly anomalies become most intense over the Equatorial Indian Ocean 10 to 15 days after the maximum MJO convective anomaly. In the SPCZ region, the mean near-surface easterlies begin to weaken at day -5, with this trend continuing through day +20. Our observations over the West Pacific are more closely linked to the findings of Agudelo et al. (2006) that suggest westerly anomalies occur closer to the time of maximum convection.

CHAPTER 6

TELECONNECTION PROCESSES

Questions still remain about what causes convection associated with the MJO to propagate in a diagonal direction along the SPCZ and how these changes in storminess influence large-scale atmospheric circulations. It has already been shown that convection in the SPCZ releases large quantities of latent heat which enhance meridional and zonal circulations (Chapter 3.2 and 3.3, respectively). We hypothesize that the significant OLR anomalies associated with MJO-SPCZ interactions are correlated with changes in local Hadley circulations and the Pacific Walker cell. These relationships are tested using a similar composite analysis to the methods discussed in Chapter 5.2. Motivations for studying variability of the Hadley and Walker circulations include understanding their roles in heat transport processes and how changes to the basic state enhance or diminish atmospheric wave propagation. We will demonstrate that understanding the latter motivation has direct consequences for answering our original question concerning what dynamical processes govern convective propagation within the SPCZ.

6.1 Wave Propagation

Matthews et al. (1996) theorize that convection over Indonesia produces a subtropical Rossby-wave response which propagates east and triggers instability in the SPCZ. This explanation does not fully clarify why MJO convection in the SPCZ is typically strongest during summer (Zhang and Dong 2004), while subtropical baroclinic instability caused by the upper tropospheric jet is greatest in winter. A likely explanation is that the low-level westerly wind burst associated with convection over Indonesia forces wave energy accumulation along the SPCZ, due to increased negative stretching deformation. It may be inferred from zonal wind anomalies that a negative stretching

deformation anomaly $\left(\frac{\partial u'}{\partial x} < 0\right)$ at the 925 hPa level would develop just east of the SPCZ, five days after the MJO convective peak over Indonesia, and continue to amplify during the following two weeks. This negative zonal stretching deformation would further amplify the accumulation of wave energy from propagating disturbances in the region (see Chapter 4.3 for a more thorough discussion of wave accumulation).

Westerly wind bursts associated with the MJO may also allow mid-latitude Rossby wave energy to propagate north into the tropical SPCZ. Webster and Holton (1982) used a non-linear shallow water model to demonstrate that mid-latitude Rossby waves have little impact on the tropics if a region of easterly winds separates the two regions. Austral summer surface easterlies (5-15ms^{-1}) extend throughout the SPCZ, except for about three weeks during and after MJO events. Cocks (2003) notes that this may explain why mid-latitude interactions with the tropical SPCZ are rare. The wavelet coherence analysis discussed in Chapter 5.1 lends credence to this theory that latitudinal interactions on sub-monthly timescales increase within the SPCZ immediately after MJO events, at least during the 2005 case study.

The MJO also seems to trigger bursts of convection in the mid-latitude SPCZ prior to the main convective envelope propagating out of the Indian Basin (Figure 5.8a, e.g., Lead 10 days). Meehl et al. (2001) proposes a mechanism where the strong tropical convection associated with the MJO triggers a mid-latitude wave train which propagates eastward with a faster velocity than the main convective region. We show an example of this mechanism in Figure 6.1. Here the wave train schematic is overlaid on OLR composite anomalies corresponding to the time of maximum MJO activity over the Indian Ocean. The schematic depicts an oscillation of high and low pressure anomalies

in the upper troposphere which arc away from the equator, over the Southern Ocean, and back into the SPCZ. The wave train may cause amplified convection well ahead of the MJO by destabilizing the atmosphere through the advection of negative vorticity (Meehl et al. 2001). Caution must be applied when considering this theory to verify that the depicted SPCZ OLR anomalies are not being triggered by a previous MJO lagging over the Central Pacific.

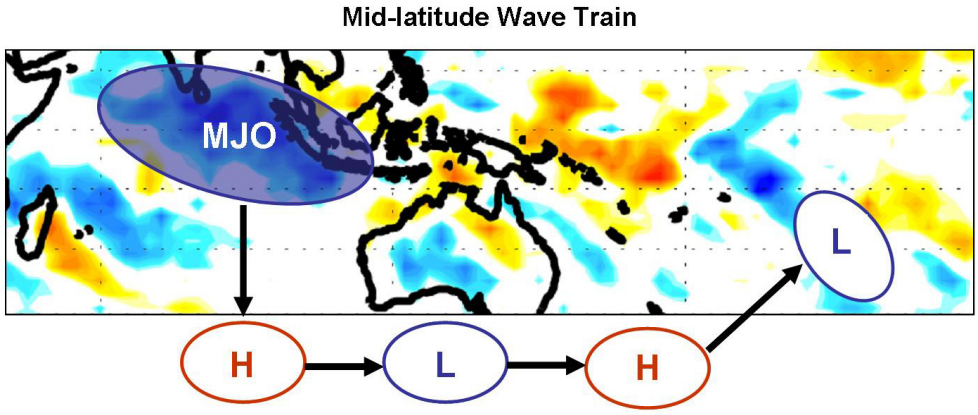

Figure 6.1 Schematic diagram of a mid-latitude wave train transferring signals from the Central Indian Ocean to the SPCZ region. Negative (positive) OLR anomalies are indicated by cool (warm) shading. H and L ellipses indicate upper tropospheric circulation anomalies. Blue shaded ellipse indicates the MJO convective envelope. Diagram adapted from Meehl et al. (2001).

6.2 Basin Scale Circulation Changes

SPCZ convection also influences interaction between the tropics and mid-latitudes on Pacific-wide spatial scales, either through changes in the strength of the Hadley circulation (Houseago-Stokes and McGregor 2000; Harangozo 2004) or by causing upper tropospheric westerly wind anomalies over the Central and Eastern Pacific.

Karoly (1989) uses composite analyses to show that the generation of Rossby waves is directly proportional to the strength of the SH Hadley circulation. Rossby waves were detected by observing wave trains of height anomalies extending from the subtropics near the dateline poleward over the South Pacific towards South America. Our climatology analysis in Chapter 3.2 suggests that the strength of vertical lift corresponds spatially with areas of deep convection. Increases in off-equatorial convection, such as in the subtropical SPCZ, relative to the local ITCZ would therefore weaken the SH Hadley circulation, decrease Rossby wave generation (Karoly 1989), and limit teleconnections across the South Pacific (Harangozo 2004).

Using the dates of MJO interaction with the SPCZ calculated in Chapter 5.2, we now discuss how the regional Hadley circulation responds to OLR anomalies on 25-80 day timescales. Figure 6.2 shows composite anomalies of the meridional circulation 15 days after maximum peaks of filtered DJF OLR values in the Indonesian region (corresponding OLR anomalies shown in Figure 5.8b). We see that vertical velocities increase over the equatorial region only when anomalous storminess is limited to the tropical latitudes, such as in the western SPCZ (Figure 6.2a). Further east (Figures 6.2b and c), the MJO is associated with off-equatorial convective anomalies and subsequent increases in vertical velocities from 10˚S-20˚S. These mass flux composites also show anomalous subsidence near the equator. Magnitudes of these anomalies are up to 20% of the DJF seasonal climatology.

Interaction of the MJO with the SPCZ also has a significant forcing on the Walker circulation. Changes in the strength and structure of equatorial zonal circulations are caused in part by fluctuations in location of tropical convective regions. The increased frequency of deep convection in the SPCZ caused by passage of MJO events results in

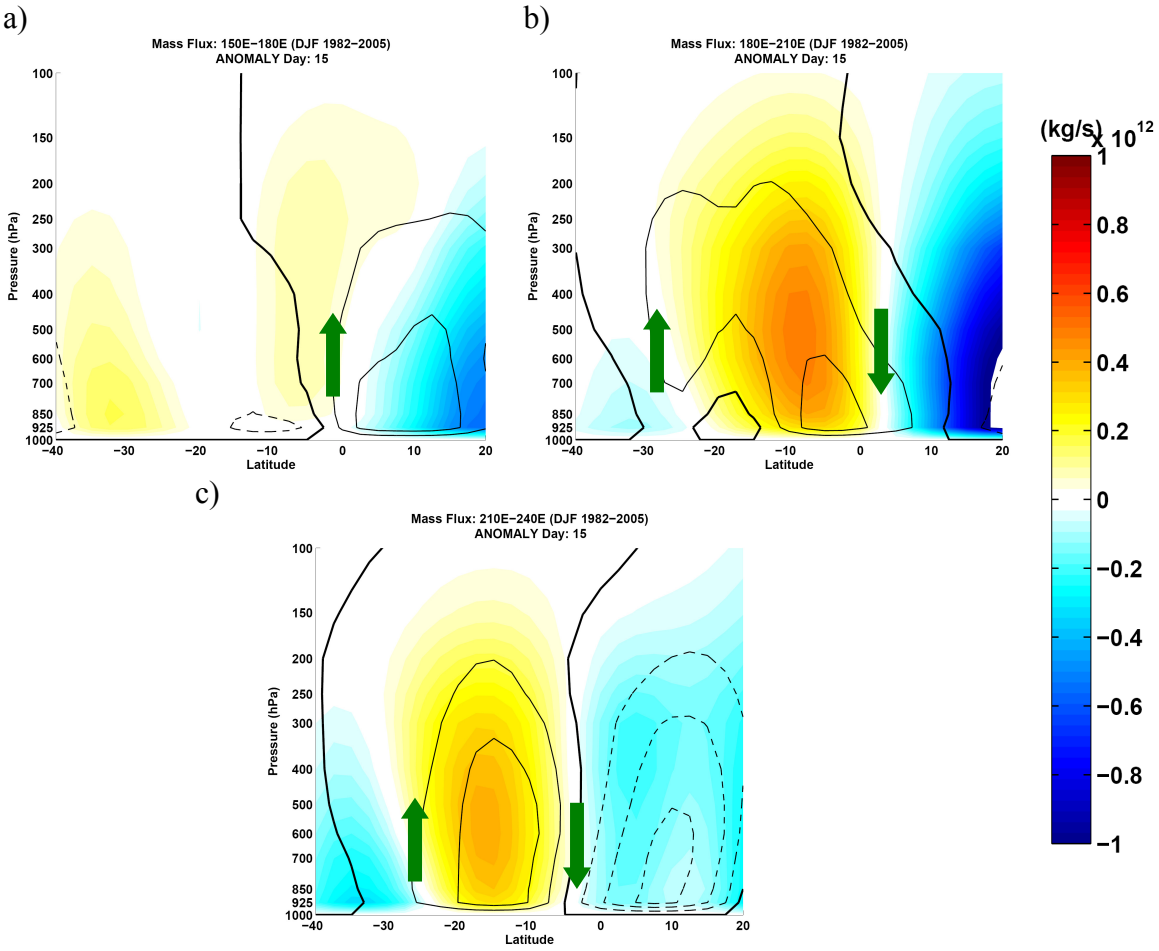

Figure 6.2 Composite anomalies of meridional cross sections of mass stream functions 15 days after the maximum peaks of filtered DJF OLR values in the Indonesian region: a) 150˚E-180˚E, b) 180˚E-210˚E, and c) 210˚E-240˚E. Austral summer climatology is indicated by shaded contours. Anomalies are shown by black contours (interval: 10^{11} kg/s, solid: positive, dashed: negative, and green arrows indicate direction). Zero anomaly contour is indicated by the thick black line.

more latent heat release in the middle and upper troposphere, leading to increased vertical ascent (Karoly and Vincent 1999). We examine how this influences the Pacific Walker cell by using a similar composite analysis to the one constructed of the local Hadley circulation response. Composite dates are again based on the time of maximum anomalous convection in the tropical SPCZ (15 days after peaks of maximum filtered

OLR values in the Indonesian region). The focus is on the DJF season as this is when both the Pacific Walker cell and SPCZ are at their maximum intensities. An additional reason for choosing this season is to better understand how convective anomalies influence the large-scale environment which governs the propagation of boreal winter mid-latitude Rossby waves into the tropics.

The zonal wind response to the passage of MJO events through the SPCZ is shown in Figure 6.3a and b. Here we observe significant low-level westerly wind anomalies throughout the tropical SPCZ during the period of enhanced MJO convection (corresponding OLR anomaly field shown in Figure 5.8b). The effects of westerly wind bursts on the zonal accumulation of wave energy near the SPCZ were discussed in Chapter 6.1. In the tropical upper troposphere, anomalies are clustered into statistically significant regions of easterlies (West Pacific) and westerlies (Central and East Pacific). These anomalies are a response to strong upper-level divergence away from clusters of deep convection.

Changes in the zonal wind flow have direct impacts on the Walker circulation. A composite anomaly of mass flux is overlaid onto the seasonal (DJF) depiction of the circulation over the Pacific Basin (Figure 6.3c). Here we see that while changes to the strength of the circulation are negligible, the locations of vertical ascent and subsidence have shifted 20˚E (indicated by the anomalous horizontal gradient of mass flux). Interaction of the MJO with the SPCZ produces increased convection between 160˚E-180˚E which becomes the location of the Pacific Walker cell's dominant rising branch. Upper level westerly anomalies are forced over the Central Pacific (Figure 6.3b) along with an eastward shift in the main region of subsidence. This supports our hypothesis that tropical circulations are strongly influenced by the location of deep convection due to the energy supplied by latent heat release from condensation.

a)

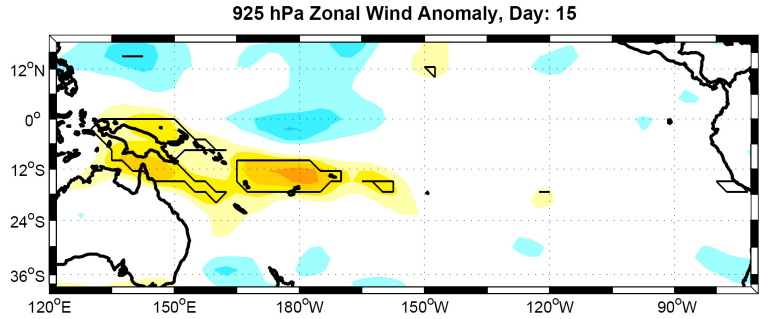

b)

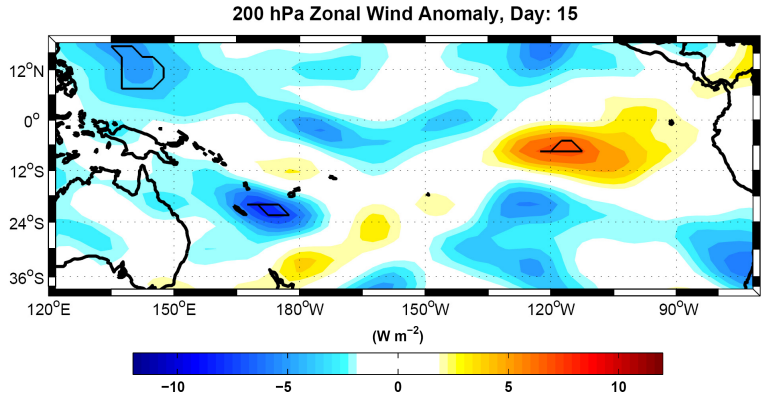

c)

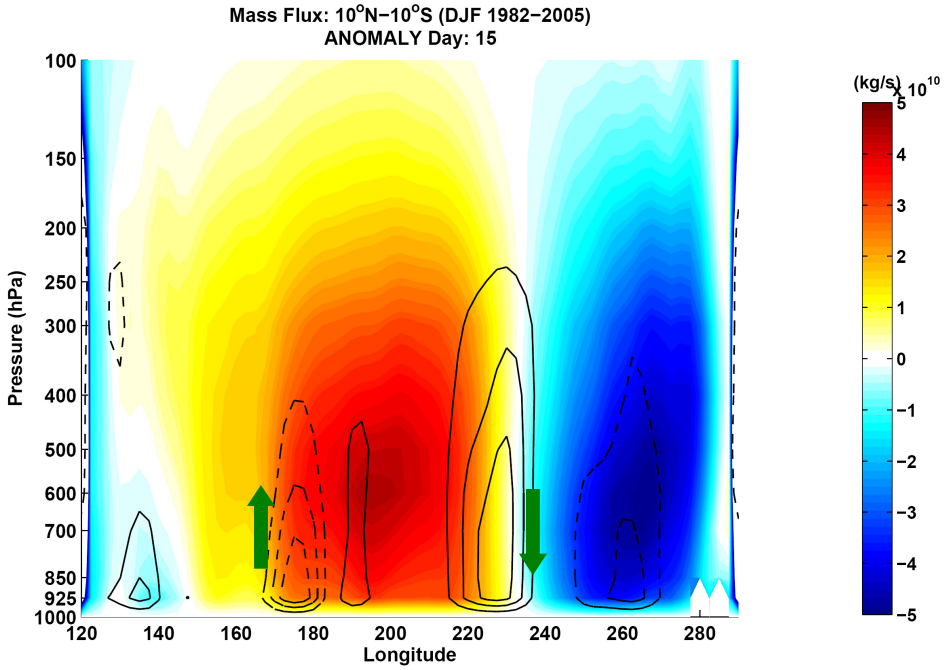

Figure 6.3 Composite anomalies of zonal winds 15 days after the maximum peaks of filtered DJF OLR values in the Indonesian region: a) 925 hPa, b) 200 hPa. Thin black lines enclose anomalies statistically significant at the 95% level. (c) Same as Figure 3.6 but with composite anomalies shown by black contours (interval: 10^{10} kg/s, solid: positive, dashed: negative, green arrows indicate direction, zero contour omitted).

Several modeling and analytical studies indicate that cross-equatorial wave propagation are dependent on the zonally varying basic state (e.g., Webster and Holton 1982; Webster and Chang 1988; Tomas and Webster 1994; Webster and Chang 1997). Webster and Holton (1982) showed that the Westerly Wind Duct of 200 hPa zonal winds over the central equatorial Pacific allows wave trains to propagate from the NH mid-latitudes into the SH. Composite anomalies show that there is a significant increase in U_{200hPa} across the tropical Central Pacific at the same time that strong DJF MJO events are interacting with the SPCZ (Figure 6.3b). These anomalies suggest that the size and intensity of the Westerly Wind Duct responds to convective patterns over the SPCZ. A larger region of westerly winds could allow mid-latitude disturbances with longer wavelengths to propagate into the tropics. The large-scale circulation connection with tropical convection therefore has important influences on inter-hemispheric and regional teleconnection processes.

CHAPTER 7

SUMMARY AND CONCLUSIONS

The ability to understand further the impacts of the SPCZ on the general atmospheric circulation and possible influences on Pacific-wide teleconnection processes is dependent on having an adequate understanding of the region. This includes not only seasonal studies of the basic state, but also information about the dynamics which spawn deep convection and govern variability of the cloud systems. From this stage, power and temporal analyses of SPCZ variability allow focus to be drawn to particular modes where improved forecast skill is possible. In this study, the significance of variability associated with sub-monthly disturbances and MJO induced convection in the SPCZ have become apparent.

7.1 Summary

Warm SSTs and abundant boundary layer moisture provide thermodynamic support for tropical SPCZ convection, especially during DJF, which has been the period of focus in this study. Strong SST gradients to the south provide baroclinic energy which supports mid-latitude cyclogenesis. Converging winds between the austral summer high pressure circulation over the South Pacific and lower pressure over the West Pacific Warm Pool further support the SPCZ by providing an environment conducive to low-level wave energy accumulation. Zonal and meridional stretching deformation suggests that energy accumulation comes from both tropical and extratropical modes. While cross-equatorial flow in the West Pacific is weaker than in monsoon circulations, the slight off-equatorial center of the SH summer SST maximum supports northerly

divergent winds as far as 10˚S. This appears to account for the advection of positive absolute vorticity into the SPCZ region, creating an inertially unstable atmosphere. Time series analysis of low-level meridional flow found numerous cross-equatorial wind bursts with 6-25 day frequencies. Composite analysis tied these events to amplified convection in the tropical and subtropical portions of the SPCZ.

Power spectra and wavelet analysis diagnostic tools of OLR time series allowed us to isolate particular triggers of convection. Coherency between the tropical and mid-latitude SPCZ is typically limited on sub-monthly scales, although the possibility exists for Rossby waves to increase interactions when the zonal flow is conducive for latitudinal propagation. Fourier decomposition was used to extract lower frequency modes of variability, such as the MJO, in order to create composites based on dates of maximum convection in the region. These OLR composites support our hypothesis that the MJO causes significant enhancement of the tropical SPCZ about three weeks after peak amplitude over the Indian Ocean. Convective bursts in the mid-latitude SPCZ prior to the main MJO convective envelope entering the region suggests a possible teleconnection route between the Indian Basin and South Pacific. Westerly wind bursts associated with the MJO also alter the basic state to allow mid-latitude Rossby wave energy to propagate equatorward into the tropical SPCZ.

Fluctuations in convection associated with the SPCZ were found to strongly influence the regional Hadley and Walker circulations. Composites showed increased vertical ascent in regions experiencing anomalous storminess. The diagonal orientation of the SPCZ leads to strong off-equatorial ascent which counteracts the classical notation of a Hadley circulation with rising air concentrated in the tropics. Rossby wave

generation is decreased during periods when the meridional circulation is weak, limiting teleconnections between tropical convection and the mid-latitude South Pacific. Anomalous SPCZ convection associated with the MJO is also correlated with a significant increase in the 200 hPa Westerly Wind Duct. This is accompanied by an eastward shift of the Pacific Walker circulation. Analytical studies have suggested that the wavelength of NH mid-latitude disturbances propagating into the SH tropics is dependent on the spatial extent of westerly winds. We therefore deduce that variability in the strength of the SPCZ influences cross-equatorial wave propagation.

7.2 Future Expansion

Questions remain about how waves grow and propagate in regions of negative meridional stretching deformation $\left(\frac{\partial v}{\partial y} < 0\right)$. Our analysis suggests that large meridional components of convergence exist along, and south of, the main SPCZ axis. We additionally found that meridional stretching becomes more negative during cross-equatorial wind bursts which also cause a significant increase in convection throughout the tropical and subtropical SPCZ. While previous modeling and analytical studies on wave responses to negative zonal stretching $\left(\frac{\partial u}{\partial x} < 0\right)$ have been conducted (e.g., Webster and Chang 1997), we are only able to hypothesize that similar energy accumulation occurs in the meridional case.

Wave responses to changes in the meridional basic state could be tested more definitively by constructing case studies to observe the propagation of individual disturbances. Here disturbances occurring in a strongly meridional stretching flow would be analyzed to determine if their group speeds decrease and wave energy accumulates.

Negative meridional stretching may also increase genesis rates of new waves. One possible mechanism for this would be that increased low-level convergence leads to anomalous convection. Waves have previously been observed to emanate from regions of latent heat release associated with deep convection in the tropics (Wheeler and Kiladis 1999).

Further analysis is necessary to diagnose why the mid-latitude SPCZ becomes amplified during periods of strong MJO convection over the Indian Ocean. We mentioned that caution must be applied to definitively linking different composite anomalies, especially without a clear dynamical explanation. Preliminary research suggests that upper tropospheric circulation anomalies arc poleward away from large regions of tropical convection and form mid-latitude wave trains. It remains uncertain whether this presents an avenue for early prediction of the SPCZ response to MJO events. For example, a definitive teleconnection relationship would mean that detection of a developing MJO could be used to forecast enhanced convection in the mid-latitude SPCZ several days later, while the MJO convective envelope is still over the Indian Basin. Prediction of anomalous off-equatorial convection has important weather forecasting applications as it would represent skill in determining the meridional circulation which has been demonstrated to influence SH Rossby wave formation (Karoly 1989).

One additional set of questions concerns long term variability of the SPCZ and regional circulation patterns. Interactions between convection and tropical SSTs suggest that a warming climate could trigger significant changes. General circulation models (GCMs) could be used to diagnose if precipitation patterns associated with the SPCZ change in response to a warming climate. Scrutiny must be applied to GCM results as

they have previously demonstrated little skill in forecasting the diagonal orientation of convection in the South Pacific (Cocks 2003). Sources of error could be mitigated if the research focus was applied strictly to measuring changes in the tropical SPCZ. Weakening of the Pacific Walker cell has recently been detected using 20th century surface pressure observations (Vecchi et al. 2006). GCM runs for the next hundred years predict an additional 10-15% weakening of this zonal circulation and suggest that it could lead to increased vertical wind shear over the Atlantic, with important consequences for TC development (Vecchi and Soden 2007). Future research is necessary to determine which physical mechanisms are involved in the predicted weakening of the Pacific Walker circulation. Possibilities include a slower rising branch due to increased evaporation and constant precipitation over the West Pacific (Held and Soden 2006), changes in the zonal SST gradient, and fluctuations in regions of deep convection. This study has demonstrated that convective variability in the South Pacific significantly impacts circulation patterns on sub-monthly and intraseasonal timescales. It remains to be seen whether similar long term interactions exist.

REFERENCES

Agudelo, P. A., J. A. Curry, C. D. Hoyos, and P. J. Webster, 2006: Transition between suppressed and active phases of intraseasonal oscillations in the Indo-Pacific warm pool. *J. Climate*, **19**, 5519-5530.

Benedict, J., 2005: The birth and death of the MJO: An observational study. M.S. thesis, Dept. of Atmospheric Science, Colorado State University, Fort Collins, CO, 131.

Cocks, S. B., 2003: An observational study of the South Pacific Convergence Zone using satellite and model re-analysis data. Ph.D. thesis, Dept. of Atmospheric Science, Texas A&M University, Galveston, TX, 155.

Cook, K., 2000: The South Indian Convergence Zone and the interannual rainfall variability over southern Africa. *J. Climate*, **13**, 3789-3804.

Cromwell, D., 2001: Sea surface height observations of the 34°N 'waveguide' in the North Atlantic. *Geophys. Res. Lett.*, **28**, 3705-3708.

Duchon, C., 1979: Lanczos filtering in one and two dimensions. *J. Appl. Meteor.*, 1016-1022.

Eastin, M. and D. Vincent, 1998: A 6-yr climatology of vertical mean and shear components of kinetic energy for the Australian-South Pacific jet stream. *J. Climate*, **11**, 283-291.

Fukutomi, Y. and T. Yasunari, 2005: Southerly surges on sub-monthly time scales over the Eastern Indian Ocean during the Southern Hemisphere winter. *Mon. Wea. Rev.*, **133**, 1637-133.

Graham, N. E. and T. P. Barnett, 1987: Sea surface temperature, surface wind divergence, and convection over tropical oceans. *Science*, **238**, 657-659.

Grinsted, A., J. Moore, and S. Jevrejeva, 2004: Application of the cross wavelet transform and wavelet coherence to geophysical time series. *Nonlinear Processes in Geophysics*, **11**, 561-566.

Gu, G.J. and C. D. Zhang, 2002: Cloud components of the Intertropical Convergence Zone. *J. Geophys. Res.-Atmospheres*, **107**, 4565.

Hannachi, A., 2004: *A primer for EOF analysis of climate data*. Department of Meteorology, University of Reading, 33.

Harangozo, S., 2004: The relationship of Pacific deep tropical convection to the winter and springtime extratropical atmospheric circulation of the South Pacific in El Niño events. *Geophys. Res. Lett.*, **31**, 1-4.

Hartmann, D. L., 1994: *Global Physical Climatology*. Academic Press, 411.

Hartmann, D. L., 2005: *Class notes: ATM 552 Objective Analysis*. Department of Atmospheric Science, University of Washington, 142.

Held, I. M. and B. J. Soden, 2006: Robust responses of the hydrological cycle to global warming. *J. Clim.*, **19**, 5686-5699.

Holton, J. R., 2004: *An introduction to dynamic meteorology, Third Edition*. Academic Press, 535.

Houseago-Stokes, R. and G. McGregor, 2000: Spatial and temporal patterns linking southern low and high latitudes during South Pacific warm and cold events. *Int. J. Climatol.*, **20**, 793-801.

Hurrell, J. and D. Vincent, 1987: Significance of the South Pacific Convergence Zone (SPCZ) in the energy budget of the Southern Hemisphere tropics. *Mon. Wea. Rev.*, **115**, 1797-1801.

Kalnay et al., 1996: The NCEP/NCAR 40-year reanalysis project. *Bull. Amer. Meteor. Soc.*, **77**, 437-470.

Karoly, D. J., 1989: Southern Hemisphere circulation features associated with El Niño-Southern Oscillation events. *J. Clim.*, **2**, 1239-1252.

Karoly, D. and D. Vincent, 1999: Meteorology of the Southern Hemisphere. *Meteor. Monogr.*, **27**, 101-117.

Kiladis, G. and M. Wheeler, 1995: Horizontal and vertical structure of observed tropospheric equatorial waves. *J. Geophys. Res.-Atmospheres*, **100**, 22981-22997.

Kiladis, G., H. Storch, H. Loon, 1989: Origin of the South-Pacific Convergence Zone. *J. Clim.*, **2**, 1185-1195.

Kistler, R., et. al., 2001: The NCEP-NCAR 50-year reanalysis: Monthly means CD-ROM and documentation. *Bull. Amer. Meteor. Soc.*, **82**, 247-267.

Kodama, Y., 1993: Large-scale common features of sub-tropical convergence zones. *J. Meteor. Soc. Japan*, **17**, 581-610.

Liebmann B. and C.A. Smith, 1996: Description of a complete (interpolated) outgoing longwave radiation dataset. *Bull. Amer. Meteor. Soc.*, **77**, 1275-1277.

Madden, R. A. and P. R. Julian, 1994: Observations of the 40-50-day tropical oscillation-A review. *Mon. Wea. Rev.*, **122**, 814-837.

Matthews, A., 2000: Propagation mechanisms for the Madden-Julian Oscillation. *Quart. J. Roy. Meteor. Soc*., **126**, 2637-2651.

Matthews, A., B. Hoskins, J. Slingo, et al., 1996: Development of convection along the SPCZ within a Madden-Julian oscillation. *Quart. J. Roy. Meteor. Soc*., **122**, 669-688.

Meehl, G. A., et. al., 2001: A conceptual framework for time and space scale interactions in the climate system. *Climate Dyn.*, **17**, 753-775.

Schnadt, C., A. Fink, D. Vincent, J. Schrage, and P. Speth, 1998: Tropical cyclones, 6-25 day oscillations, and tropical-extratropical interaction over the Northwestern Pacific. *Meteorol. Atmos. Phys.*, **68**, 151-169.

Streten, N., 1973: Some characteristics of satellite-observed bands of persistent cloudiness over the Southern Hemisphere. *Mon. Wea. Rev.*, **6**, 486-495.

Torrence, C., and G. Compo, 1998: A practical guide to wavelet analysis. *Bull. Amer. Meteor. Soc.*, **79**, 61-78.

Tomas, R. and P. J. Webster, 1994: Horizontal and vertical structure of cross-equatorial wave propagation. *J. Atmos. Sci.,* **51**, 1417-1429.

Tomas, R. and P. J. Webster, 1997: The role of inertial instability in determining the location and strength of near-equatorial convection. *Quart. J. Roy. Meteor. Soc*., **123**, 1445-1482.

Tomas, R., R. Holton, and P. J. Webster, 1999: The influence of cross-equatorial pressure gradients on the location of near-equatorial convection. *Quart. J. Roy. Meteor. Soc*., **125**, 1107-1127.

Trenberth, K., 1976: Spatial and temporal variations of the Southern Oscillation. *Quart. J. Roy. Meteor. Soc*., **102**, 639-653.

Trenberth, K., 1997: The definition of El Niño. *Bull. Amer. Meteor. Soc.*, **78**, 2771-2777.

Vecchi, G. A. and B. J. Soden, 2007: Increased tropical Atlantic wind shear in model projections of global warming. *Geophys. Res. Lett.*, **34**, 1-5.

Vecchi, G. A. et al., 2006: Weakening of tropical Pacific atmospheric circulation due to anthropogenic forcing. *Nature*, **441**, 73-76.

Vincent, D., 1994: The South Pacific convergence zone (SPCZ): A review. *Mon. Wea. Rev.,* **122**, 1949-1970.

Webster, P. J. and J. R. Holton, 1982: Cross-equatorial response to middle-latitude forcing in a zonally varying basic state. *J. Atmos. Sci.*, **39**, 722-733.

Webster, P. J. and H. R. Chang, 1988: Equatorial energy accumulation and emanation regions: Impacts of a zonally varying basic state. *J. Atmos. Sci.*, **45,** 803-829.

Webster, P. J. and H. R. Chang, 1997: Atmospheric wave propagation in heterogeneous flow: basic flow controls on tropical-extratropical interaction and equatorial wave modification. *Dyn. Atmos. Oceans*, **27**, 91-134.

Webster, P. J., V. O. Magana, T. N. Palmer, J. Shukla, R. A. Tomas, M. Yanai, and T. Yasunari, 1998: Monsoons: Processes, predictability, and the prospects for prediction. *J. Geophys. Res.*, **103**, 14,451-14,510.

Wheeler, M. and G. Kiladis, 1999: Convectively coupled equatorial waves: Analysis of clouds and temperature in the wavenumber-frequency domain. *J. Atmos. Sci.*, **56**, 374-399.

Wheeler, M. and K. Weickmann, 2001: Real-time monitoring and prediction of modes of coherent synoptic to intraseasonal tropical variability. *Bull. Amer. Meteor. Soc.*, **129**, 2677-2694.

Wilks, D. S., 1995: *Statistical methods in the atmospheric sciences*. Academic Press, 467.

Yoshikane, T. and F. Kimura, 2003: Formation mechanism of the simulated SPCZ and Baiu front using a regional climate model. *J. Atmos. Sci.*, **60**, 2612-2632.

Zhang, C. and P. J. Webster, 1989: Effects of zonal forcing on equatorially trapped waves. *J. Atmos. Sci.*, **46**, 3632-3652.

Zhang, C. and M. Dong, 2004: Seasonality in the Madden-Julian Oscillation. *J. Clim.*, **17**, 3169-3180.